iScience

CellPress

Article

Chromatin Succinylation Correlates with Active Gene Expression and Is Perturbed by Defective TCA Cycle Metabolism

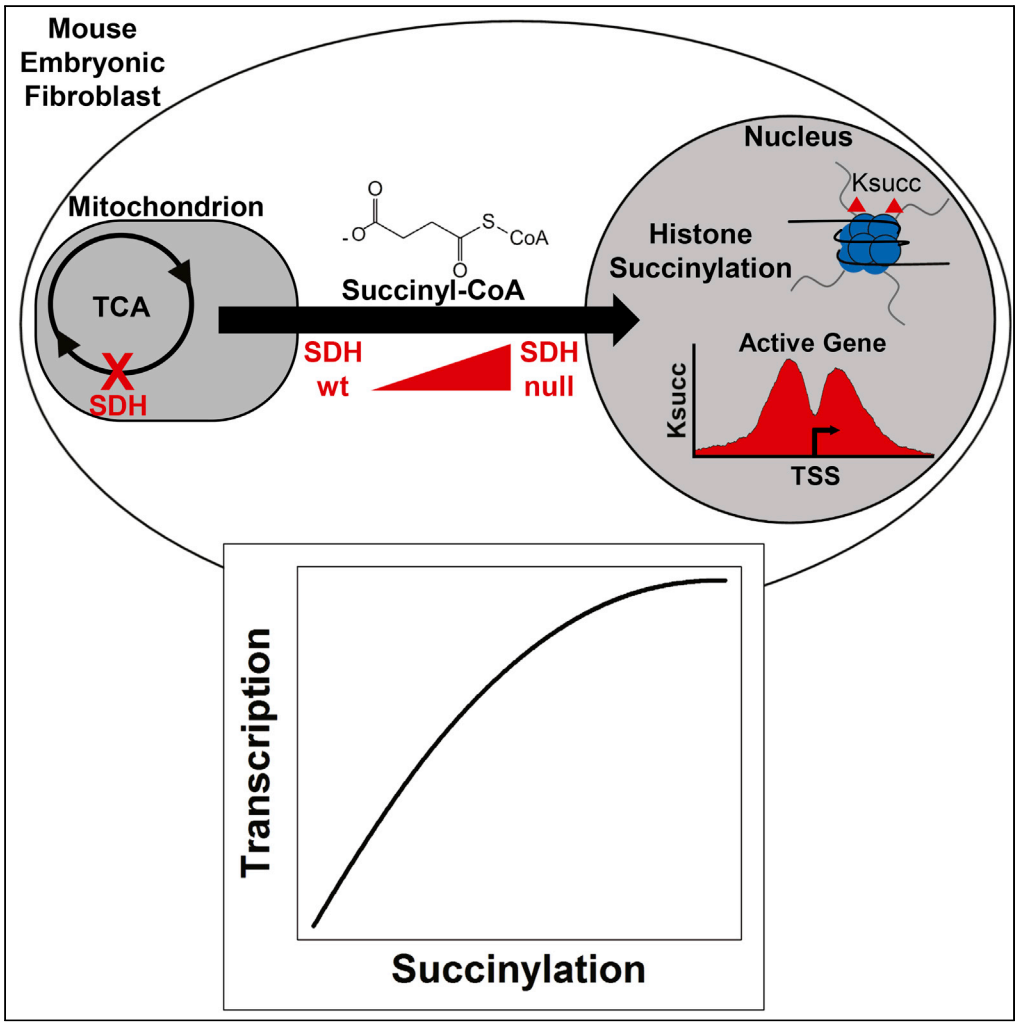

John Smestad, Luke Erber, Yue Chen, L. James Maher III

maher@mayo.edu

HIGHLIGHTS

SDH loss TCA cycle defect results in succinyl-CoA increase and hypersuccinylation

Succinyllysine modification of chromatin correlates with active gene expression

Chromatin succinyllysine change in SDH loss correlates with transcriptional change

Smestad et al., iScience 2, 63–75
April 27, 2018
https://doi.org/10.1016/j.isci.2018.03.012

iScience

CellPress

Article

Chromatin Succinylation Correlates with Active Gene Expression and Is Perturbed by Defective TCA Cycle Metabolism

John Smestad,[1,2] Luke Erber,[3] Yue Chen,[3] and L. James Maher III[2,4,*]

SUMMARY

Succinylation is a post-translational protein acylation modification that converts the cationic lysine side chain to an anion with large potential impacts on protein structure and function. Here we characterize the epigenome-wide distribution of succinyllysine marks in chromatin using chromatin immunoprecipitation sequencing (ChIP-seq). We estimate that more than one-third of all nucleosomes contain lysine succinylation marks and demonstrate a potential role of chromatin succinylation in modulating gene expression. We further demonstrate that defective tricarboxylic acid (TCA) cycle metabolism perturbs the succinyllysine distribution in chromatin, correlating with transcriptional responses. This is consistent with previous observations linking nucleosome succinylation with enhanced *in vitro* transcription. We additionally demonstrate that defective TCA cycle metabolism results in a DNA repair defect and sensitivity to genotoxic agents, consistent with previously reported chromatin hypersuccinylation effects observed in the context of SIRT7 depletion. Chromatin succinylation may thus represent a mechanism by which metabolism modulates both genome-wide transcription and DNA repair activities.

INTRODUCTION

Lysine succinylation (Figure 1A [Zhang et al., 2011]) has emerged as a novel post-translational modification (PTM) that directly couples tricarboxylic acid (TCA) cycle metabolism, via succinyl-CoA, to alterations in the charges, structures, and activities of proteins involved in diverse cellular processes. Global proteomic approaches have revealed that the lysine succinylome spans multiple biological compartments, including the nucleus, but with concentrated effects in the mitochondria (Park et al., 2013). Succinylation is one of many known acyl modifications capable of decorating the lysine residues in proteins, with others including acetylation, propionylation, malonylation, crotonylation, butyrylation, glutarylation, 2-hydroxyisobutyrylation, and β-hydroxybutyrylation (Chen et al., 2007; Choudhary et al., 2009; Dai et al., 2014; Du et al., 2011; Garrity et al., 2007; Tan et al., 2011, 2014; Xie et al., 2016).

Significant discussion persists within the field regarding whether the attachment of the various acyl PTMs to lysine residues is enzyme mediated. Acetylation is the oldest known and best studied acyl PTM, and many acetyltransferases and deacetylases catalyzing the attachment and removal of acetyl marks, respectively, have been identified (Ito et al., 2000; McManus and Hendzel, 2000; Michishita et al., 2008; Ravindra et al., 2009; Tafrova and Tafrov, 2014; Warrener et al., 2010; Xiong et al., 2010; Yang et al., 2011; Zhang et al., 1998). Several acetyltransferases have also been identified that promiscuously attach propionyl and butyryl groups to lysine residues (Leemhuis et al., 2008; Simithy et al., 2017). It remains less clear whether other acyl PTMs are attached to lysine residues in an enzyme-mediated manner. Recent work has suggested that several of the larger acyl modifications such as succinylation, malonylation, crotonylation, glutarylation, and β-hydroxybutyrylation may predominantly functionalize proteins via a non-enzymatic mechanism (Simithy et al., 2017; Wagner et al., 2017). This suggests that the rates of attachment for the various acyl-CoA species to lysine residues may be primarily governed by the concentrations of the involved reactants.

In contrast to the current paradigm of non-enzymatic succinylation, the process of desuccinylation may be mediated by specific enzymes. SIRT5 has been identified as a lysine desuccinylase that catalyzes the removal of succinyl marks from lysine residues in the mitochondria and cytoplasm (Du et al., 2011). Attenuation of SIRT5 alters the distribution of lysine succinylation marks (Park et al., 2013; Rardin et al., 2013). Importantly, depletion of SIRT5 has been shown to impair the function of complex II

[1]Mayo Clinic Medical Scientist Training Program, Mayo Clinic College of Medicine and Science, 200 1st St SW, Rochester, MN 55905, USA

[2]Department of Biochemistry and Molecular Biology, Mayo Clinic College of Medicine and Science, 200 1st St SW, Rochester, MN 55905, USA

[3]Department of Biochemistry, Molecular Biology and Biophysics, University of Minnesota at Twin Cities, Minneapolis, MN 55455, USA

[4]Lead Contact

*Correspondence: maher@mayo.edu

https://doi.org/10.1016/j.isci.2018.03.012

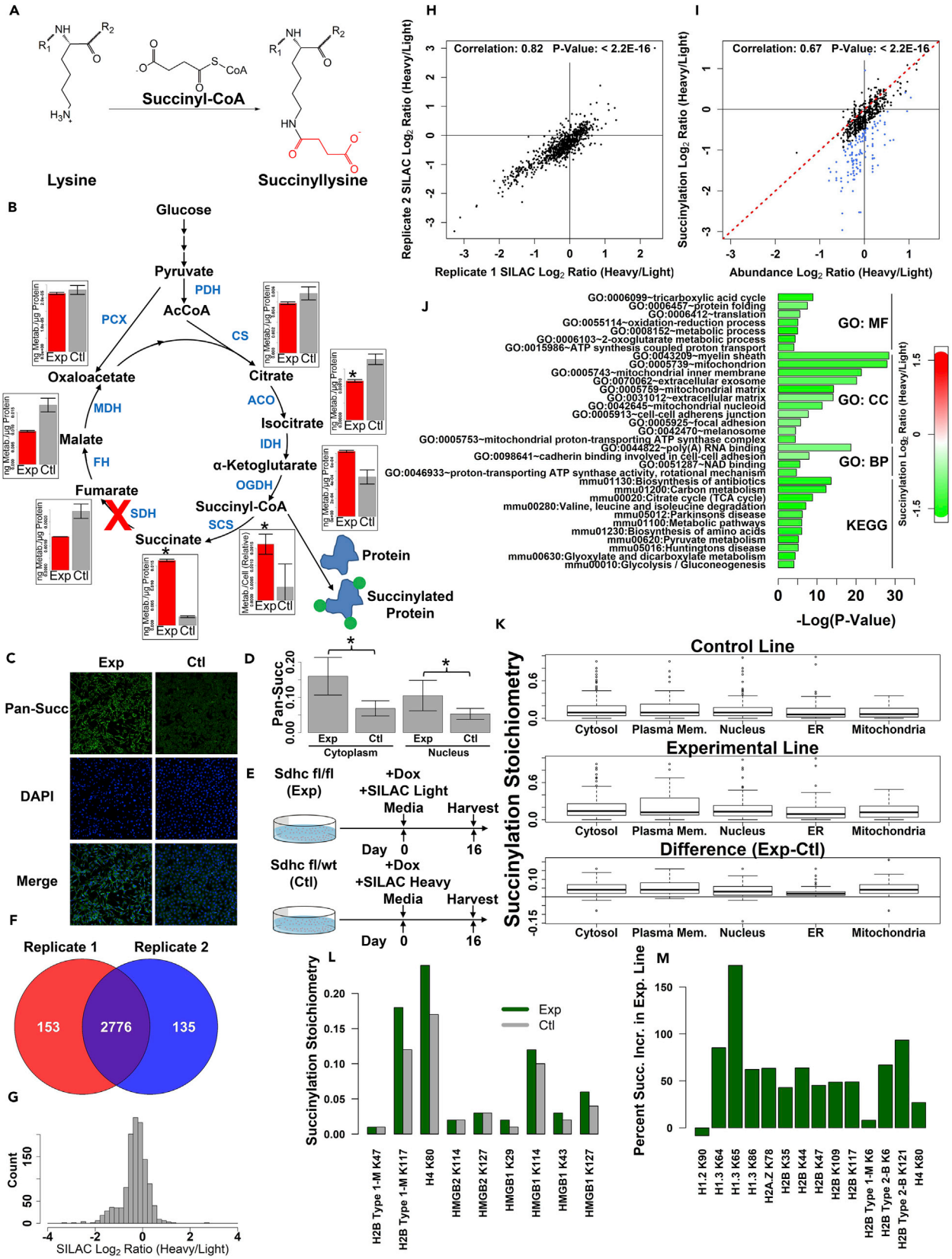
A
Succinyl-CoA
Lysine
Succinyllysine
B
Glucose
Pyruvate
PDH
PCX
AcCoA
CS
Oxaloacetate
Citrate
ACO
MDH
Isocitrate
Malate
IDH
FH
α-Ketoglutarate
Fumarate
OGDH
SDH
Succinyl-CoA
SCS
Succinate
Protein
Succinylated Protein
Exp Ctl
C
Exp
Ctl
Pan-Succ
DAPI
Merge
D
Pan-Succ
Cytoplasm
Nucleus
E
Sdhc fl/fl (Exp)
+Dox
+SILAC Light
Media
Harvest
Day 0
16
Sdhc fl/wt (Ctl)
+Dox
+SILAC Heavy
Media
Harvest
Day 0
16
F
Replicate 1
Replicate 2
153
2776
135
G
Count
SILAC Log2 Ratio (Heavy/Light)
H
Correlation: 0.82 P-Value: < 2.2E-16
Replicate 2 SILAC Log2 Ratio (Heavy/Light)
Replicate 1 SILAC Log2 Ratio (Heavy/Light)
I
Correlation: 0.67 P-Value: < 2.2E-16
Succinylation Log2 Ratio (Heavy/Light)
Abundance Log2 Ratio (Heavy/Light)
J
GO:0006099~tricarboxylic acid cycle
GO:0006457~protein folding
GO:0006412~translation
GO:0055114~oxidation-reduction process
GO:0008152~metabolic process
GO:0006103~2-oxoglutarate metabolic process
GO:0015986~ATP synthesis coupled proton transport
GO:0043209~myelin sheath
GO:0005739~mitochondrion
GO:0005743~mitochondrial inner membrane
GO:0070062~extracellular exosome
GO:0005759~mitochondrial matrix
GO:0031012~extracellular matrix
GO:0042645~mitochondrial nucleoid
GO:0005913~cell-cell adherens junction
GO:0005925~focal adhesion
GO:0042470~melanosome
GO:0005753~mitochondrial proton-transporting ATP synthase complex
GO:0044822~poly(A) RNA binding
GO:0098641~cadherin binding involved in cell-cell adhesion
GO:0051287~NAD binding
GO:0046933~proton-transporting ATP synthase activity, rotational mechanism
mmu01130:Biosynthesis of antibiotics
mmu01200:Carbon metabolism
mmu00020:Citrate cycle (TCA cycle)
mmu00280:Valine, leucine and isoleucine degradation
mmu05012:Parkinsons disease
mmu01100:Metabolic pathways
mmu01230:Biosynthesis of amino acids
mmu00620:Pyruvate metabolism
mmu05016:Huntingtons disease
mmu00630:Glyoxylate and dicarboxylate metabolism
mmu00010:Glycolysis / Gluconeogenesis
GO: MF
GO: CC
GO: BP
KEGG
Succinylation Log2 Ratio (Heavy/Light)
-Log(P-Value)
K
Control Line
Experimental Line
Difference (Exp-Ctl)
Succinylation Stoichiometry
Cytosol
Plasma Mem.
Nucleus
ER
Mitochondria
L
Succinylation Stoichiometry
Exp
Ctl
H2B Type 1-M K47
H2B Type 1-M K117
H4 K80
HMGB2 K114
HMGB2 K127
HMGB1 K29
HMGB1 K114
HMGB1 K43
HMGB1 K127
M
Percent Succ. Incr. in Exp. Line
H1.2 K90
H1.3 K64
H1.3 K65
H1.3 K86
H2A.Z K78
H2B K35
H2B K44
H2B K47
H2B K109
H2B K117
H2B Type 1-M K6
H2B Type 2-B K6
H2B Type 2-B K121
H4 K80

Figure 1. Global Lysine Succinylation Affects Multiple Cellular Compartments and Is Perturbed in the Context of SDH Loss

(A) Reaction of the ε-amino group of lysine with succinyl-CoA to form succinyllysine.

(B) TCA cycle metabolism and succinyl-CoA as a protein succinylating agent. Also shown are TCA cycle metabolites quantified for *Sdhc* fl/fl (experimental) and *Sdhc* fl/wt (control) cells 16 days after induction of *Sdhc* gene rearrangement with the doxycycline-inducible tetOcre system. Error bars indicate measurement standard deviations. Asterisks indicate comparisons that were statistically significant (p value < 0.05) by heteroscedastic 1-tailed t test.

(C) Pan-succinyllysine immunostaining of experimental and control cell lines.

(D) Quantification of mean cytoplasmic and nuclear pan-succinyllysine immunostaining intensity. Asterisks indicate degree of statistical significance by heteroscedastic 1-tailed t test (*p value < 2.2×10^{-16}).

(E) Schematic of experimental design to assess differential protein succinylation in the context of SDHC loss. TetOcre-mediated *Sdhc* gene rearrangement is induced on day 0 by doxycycline. On the same day, *Sdhc* fl/fl (experimental) cells are transitioned to SILAC light media and *Sdhc* fl/+ (control) cells are transitioned to SILAC heavy media containing isotopically labeled lysine and arginine.

(F) Overlap of succinylated sites quantified between two biological replicates.

(G) Distribution of SILAC $\log_2$ ratios of heavy and light peptides (averaged between replicate experiments).

(H) Spearman correlation analysis of site succinylation values from two biological replicates.

(I) Analysis of correlation between protein succinylation change (y axis) and protein abundance change (x axis). Subset of data points for which succinylation $\log_2$ ratio and abundance $\log_2$ ratio differed by more than 0.2 is highlighted in blue.

(J) Analysis of gene ontologies and KEGG pathways preferentially affected by differential protein succinylation in the context of SDHC loss. Terms are grouped according to ontology (MF, molecular function; CC, cellular component; BP, biological process) or KEGG pathway. Color reflects the average succinylation $\log_2$(fold-change) for identified proteins mapping to a given term [green, negative heavy/light $\log_2$(fold-change) and increased succinylation in SDHC loss]. See also Figure S1.

(K) Box plot showing succinylation stoichiometries (fraction of a given protein site that is succinylated) for proteins quantified in experimental and control cell lines, separated according to intracellular compartment. See also Figure S1.

(L) Succinylation stoichiometries for histone and non-histone chromatin proteins quantified in experimental (green) and control (gray) cell lines.

(M) Relative percent increase in histone protein succinylation quantified between experimental and control cell lines.

(succinate dehydrogenase [SDH]) and fatty acid β-oxidation, suggesting that succinylation inhibits mitochondrial enzymes (Park et al., 2013; Rardin et al., 2013). Recent work has extended these observations by identifying SIRT5 as an important regulator of cardiomyocyte biology via modulation of hydroxyacyl-CoA dehydrogenase trifunctional multienzyme complex subunit alpha (HADHA/ECHA) activity, a protein involved in fatty acid β-oxidation (Sadhukhan et al., 2016). These findings imply that lysine succinylation modulates enzyme activity in a previously unappreciated layer of biological regulation.

Initial reports of succinylation PTMs also included lysine succinylation of histones (Xie et al., 2012). These early studies revealed specific succinylation sites and characterized loss of yeast viability resulting from mutation of histone residues that are normally highly succinylated. These results suggested that histone succinylation is important for cell viability. Although provocative, the basis for these findings has remained unclear, and the relevance of histone succinylation for biological regulation has been uncertain. More recent work identified SIRT7 as a nuclear-localizing histone desuccinylase that functionally links the poly (ADP-ribose) polymerase (PARP) 1-dependent DNA damage response and chromatin compaction essential for cell survival following genotoxic stress (Li et al., 2016). A high priority for the field is to characterize other functions of histone lysine succinylation in regulating nuclear processes such as transcription.

We have been interested in the possibility that disease-causing TCA cycle defects may affect the lysine succinylome and contribute to pathologic processes. In the present work, we characterize succinylation in an inducible cell culture model of SDH loss, which results in accumulation of succinate and succinyl-CoA. This allowed us to characterize perturbation of the lysine succinylome relevant to several human malignancies including paraganglioma/pheochromocytoma (PPGL), gastrointestinal stromal tumor (GIST), renal cell carcinoma (RCC), thyroid cancer, and colon cancer (Agaimy, 2016; Astuti et al., 2001; Baysal et al., 2000; Gill et al., 2013; Nannini et al., 2014; Ni et al., 2015; Niemann and Müller, 2000; Pantaleo et al., 2015; Wang et al., 2016).

Our analyses reveal succinylation effects in several subcellular compartments, including histone and non-histone chromatin components in the nucleus. We characterize for the first time the epigenome-wide distribution of succinyllysine marks in chromatin using chromatin immunoprecipitation sequencing (ChIP-seq), revealing a potential role of chromatin succinylation in modulating gene expression. In addition, we analyze epigenome-wide patterns of chromatin succinylation perturbation in the context of SDH loss and document correlations with altered gene expression. These results are consistent with previous observations linking nucleosome succinylation with enhanced *in vitro* transcription. We also demonstrate that

defective TCA cycle metabolism results in a DNA repair defect and sensitivity to genotoxic agents, consistent with previously reported chromatin hypersuccinylation effects observed in the context of SIRT7 depletion. Chromatin succinylation may thus represent a mechanism by which metabolism modulates both genome-wide transcription and DNA repair activities.

RESULTS

SDH Loss Leads to Global Lysine Hypersuccinylation in Multiple Subcellular Compartments, Especially Mitochondria

Biallelic loss of genes encoding subunits of the SDH complex in the TCA cycle results in accumulation of succinate and succinyl-CoA (Figure 1B). Previous work has shown that these metabolic effects are only observed in the context of homozygous SDH subunit depletion, with no evidence for metabolic abnormalities in hemizygous lines (Smestad et al., 2017). We therefore hypothesized that a global hypersuccinylation effect might be observed in the context of SDH loss due to accumulation of succinyl-CoA, the presumptive succinylating agent. We therefore performed immunostaining using an anti-succinyllysine antibody (PTM-401) to assess whether SDH loss results in an observable bulk protein hypersuccinylation effect (Figure 1C). Intriguingly, hypersuccinylation effects were observable both in the cytoplasm and the nucleus of SDH loss cells, but with most effects observable in the cytoplasm (Figure 1D). This inspired us to perform a more granular analysis of protein-specific hypersuccinylation effects. We therefore performed stable isotope labeling with amino acids in cell culture (SILAC) labeling of SDH knockout (SILAC light) and control (SILAC heavy) immortalized mouse embryonic fibroblast (iMEF) cell lines using ^{13}C-labeled lysine and arginine followed by global proteomic analysis of succinylated peptides purified by immunoprecipitation (Figure 1E). Specificity of the anti-succinyllysine antibody (PTM-401) was confirmed by analysis of the prevalence of succinyllysine and the various other acyl modifications in the antibody-enriched peptide pool (Figure S1A). Analysis of biological replicate experiments identified 2,776 unique succinylation sites, yielding quantifiable SILAC heavy/light ratios between replicates (Figure 1F, Table S1). Following succinylation site identification and quantification, distributions of median-normalized SILAC heavy/light ratios were $\log_2$-transformed, revealing a non-Gaussian distribution of SILAC $\log_2$ ratios with hypersuccinylation in the SDH loss cell line as hypothesized (Figure 1G). Analysis of the correlation between $\log_2$-transformed SILAC heavy/light ratios in biological replicates (Figure 1H) confirmed reproducibility (Spearman correlation coefficient: 0.82; p value $< 2.2 \times 10^{-16}$).

As SDH loss may alter both protein abundance and protein lysine succinylation, we identified proteins whose change in lysine succinylation was disproportionate to their change in abundance upon SDH loss (Figure 1I). This analysis identified 78 such cases (Table S2). Matching gene ontologies and KEGG pathways associated with this set of proteins demonstrated a hypersuccinylation effect concentrated in the mitochondria, but that is detectable in several other cellular compartments (Figure 1J). Analysis of mitochondrial proteins in this differentially succinylated subset revealed dramatic effects for proteins involved in glycolysis/TCA cycle, fatty acid catabolism, ketone body metabolism, heat shock response, solute transport, ATP synthesis, amino acid synthesis, and the electron transport chain (Figure S1B). Protein hypersuccinylation affecting multiple subcellular compartments in the context of SDH loss had not previously been reported. It is possible that hypersuccinylation may contribute to suppression of mitochondrial enzymatic activities in the context of SDH loss, similar to what has been previously described in the context of SIRT5 desuccinylase knockout (Park et al., 2013).

We next assessed the degree to which particular lysine residues are succinylated. A global proteomic analysis of peptide abundance was leveraged to determine stoichiometries of succinylated and unmodified peptides (Olsen et al., 2010). A sample of 363 sites was identified with adequate abundance for this calculation, yielding succinylation stoichiometries for both SDH loss and control cells (Table S3). Mean succinylation stoichiometries were 0.13 and 0.18, respectively, for control and experimental lines (Figures S1C–S1E), demonstrating succinylation to be a high-abundance PTM and confirming the bulk increase in lysine succinylation in the context of SDH loss (Figure S1E). Intriguingly, there is a strong correlation between the extent of succinylation in the control cell line and hypersuccinylation upon SDH loss (Figure S1F). Classification of proteins based upon observed subcellular localization patterns using data from the Cell Atlas (Thul et al., 2017) revealed that both normal succinylation and hypersuccinylation induced by SDH loss are detected in most subcellular compartments (Figure 1K). We were particularly intrigued that these effects were apparent in the nucleus, as was also seen in our anti-succinyllysine immunostaining analysis (Figures 1C and 1D). We further pursued this observation.

Lysine Succinylation of Chromatin Proteins Is Common and Increases upon SDH Loss

We extracted succinylation data for all histone and non-histone chromatin components and examined the absolute impact of SDH loss on succinylation stoichiometry (Figure 1L) and relative succinylation ratio (Figure 1M). Intriguingly, several sites displayed high baseline succinylation in control cells, with increased succinylation upon SDH loss. Importantly, 17% of histone H4K80 residues were succinylated in control cells. Since two copies of histone H4 are present in each nucleosome, this suggests that perhaps one-third of all nucleosomes contain at least one succinyl mark at H4K80. In the context of SDH loss, the fraction of H4K80 residues bearing succinylation marks increases to 0.24, indicating that this already highly abundant mark increases by a further 41%. This striking prevalence of histone succinylation suggests that succinylation of chromatin components may be important for regulating nuclear functions, including chromatin dynamics and transcription.

Genome-wide Chromatin Succinylation Correlates with Euchromatic Histone Marks

We hypothesized that succinylation of histones and other chromatin components encodes regulatory information and therefore that succinyllysine marks would be non-uniformly distributed across the genome. To test this hypothesis, we mapped the genome-wide distribution of succinyllysine marks in chromatin from control and SDH-loss iMEF cell lines using a ChIP-seq approach with a pan-succinyllysine antibody, comparing the pattern of DNA sequence enrichment to patterns observed for chromatin marks commonly found in euchromatic (H3K4me3) or heterochromatic (H3K27me3) regions. Following MNase digestion and sonication, gel quantification of input chromatin fragments showed the chromatin to have an approximately mononucleosomal size distribution (Figure S2A), as did our analysis of mapped read lengths from paired-end read alignment following chromatin immunoprecipitation (ChIP) experiments involving formaldehyde cross-linking (Figure S2B). Quantified yields from ChIP experiments ranged between 0.4% and 4% (Figure S2C). Comparison of mapped reads from ChIP-seq experiments with input controls using an unbiased peak-calling algorithm identified several thousand peaks for each antibody (Figure 2A), with an average succinyllysine ChIP peak width less than 500 bp (Figure S2D). Analysis of the genome-wide distributions of identified ChIP-seq peaks revealed that the most common pattern of localization is in the intergenic regions (56%), followed by the introns (25%) and gene promoters (15% within 3 kbp of a transcription start site [TSS], 11.4% within 1 kbp of a TSS) (Figures 2B and 2C). Compared to a distribution of randomly selected genomic coordinates, this represents significant enrichment for promoter-localizing peaks (6% within 3 kbp of a TSS, 2% within 1 kbp of a TSS) as opposed to what chance would have predicted (Figure 2B), suggesting that succinyllysine marks in chromatin may play a role in transcriptional regulation.

Analysis of succinyllysine peaks between two biological replicate experiments showed high reproducibility (Pearson correlation coefficient: 0.88; p value $< 2.2 \times 10^{-16}$; Figure 2D), suggesting that the positions and intensities of chromatin succinylation are biologically stable. We compared succinyllysine locations to euchromatic histone mark H3K4me3 and heterochromatic mark H3K27me3. Intriguingly, positions of succinyllysine marks correlate positively with euchromatic H3K4me3 marks (Spearman correlation coefficient: 0.23; p value $< 2.2 \times 10^{-16}$) and correlate negatively with H3K27me3 heterochromatic marks (Spearman correlation coefficient: −0.30; p value $< 2.2 \times 10^{-16}$) (Figure 2E). This is the first evidence that chromatin lysine succinylation is a euchromatic mark (see also Figure 2F).

Chromatin Succinyllysine Marks Form a Distinctive Pattern Near Gene Promoters

We next assessed the pattern of promoter chromatin succinylation to discern any potential role in regulating gene transcription. We generated aligned probe plots (Figure 3A) and average probe plots (Figure 3B) displaying the abundance of identified peaks as a function of distance from the annotated TSS. Intriguingly, succinyllysine modification displays a distinctive pattern of enrichment peaking 600 bp upstream and downstream of the TSS, with relative depletion at the TSS and beyond 600 bp from the TSS. This pattern is clearly distinct from those observed for H4K3me3 and H3K27me3, suggesting that promoter succinylation encodes additional gene regulatory signals.

Chromatin Succinylation in Promoters Correlates with Activating Histone Marks

We assessed whether succinylation in gene promoters (4-kbp window centered on the TSS) correlates with histone marks associated with actively transcribed (H3K4me3) or epigenetically repressed (H3K27me3) genes. Intriguingly, succinyllysine marks mapped to gene promoters were found to correlate positively with H3K4me3 marks (Pearson correlation coefficient: 0.38; p value $< 2.2 \times 10^{-16}$) and correlate negatively

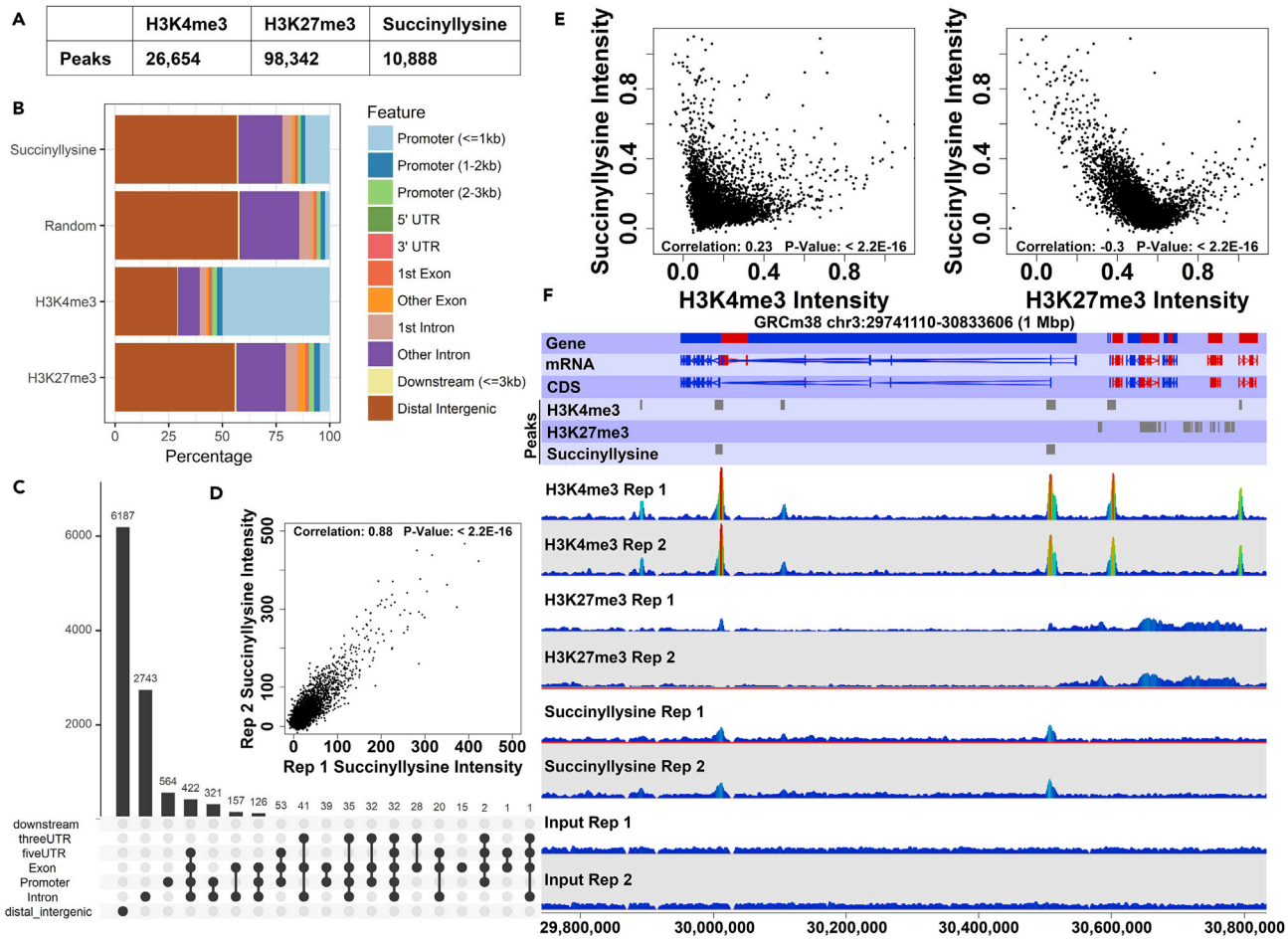

Figure 2. Succinyllysine ChIP-Seq Peaks Correlate with Euchromatic Histone Marks

(A) Numbers of peaks for each ChIP-seq target identified via the MACS peak-calling algorithm. See also Figures S2.

(B) Genomic feature localization for identified peaks. x Axis indicates percentage of identified peaks for each immunoprecipitation mapping to a given feature type.

(C) Detailed analysis of succinyllysine peak localization. Dot plot indicates genomic feature peak localization pattern, with a solid line joining two or more dots indicating instances of peaks spanning one or more genomic feature type. Bar plot above dot plot indicates number of peaks represented by a given pattern.

(D) Correlation between input-subtracted succinyllysine peak intensities quantified between ChIP-seq biological replicates.

(E) Correlation between succinyllysine signal intensity and intensities of known histone marks (H3K4me3 and H3K27me3) at positions of identified succinyllysine peaks.

(F) Representative genomic view of mouse chromosome 3 showing several identified peaks for each ChIP-seq experiment. Shown are genomic annotations for genes, mRNAs, coding DNA sequences (CDS), identified ChIP-seq peaks, and wiggle plot representations of mapped reads from the various ChIP-seq experiments. For each experiment type, mapped reads for two biological replicates are shown.

with H3K27me3 marks (Pearson correlation coefficient: −0.12; p value < 2.2×10^{-16}; Figure 3C). This coincidence of succinyl marks in chromatin with H3K4me3, but not with H3K27me3, suggests that succinylation of chromatin at active gene promoters is functionally meaningful.

Chromatin Succinylation Is a Feature of Highly Expressed Genes

We directly tested the correlation between gene expression and bulk succinylation of chromatin at gene promoters using previously published transcriptomic data for our iMEF cell lines. We identified a meaningful correlation between gene promoter chromatin succinylation and gene expression (Pearson correlation coefficient: 0.32; p value < 2.2×10^{-16}; Figure 3D), comparable to the relationship observed for H3K4me3. This is a highly provocative observation suggesting that chromatin succinylation may play a functional role in transcriptional regulation. Intriguingly, previous *in vitro* studies have shown that bulk and non-specific

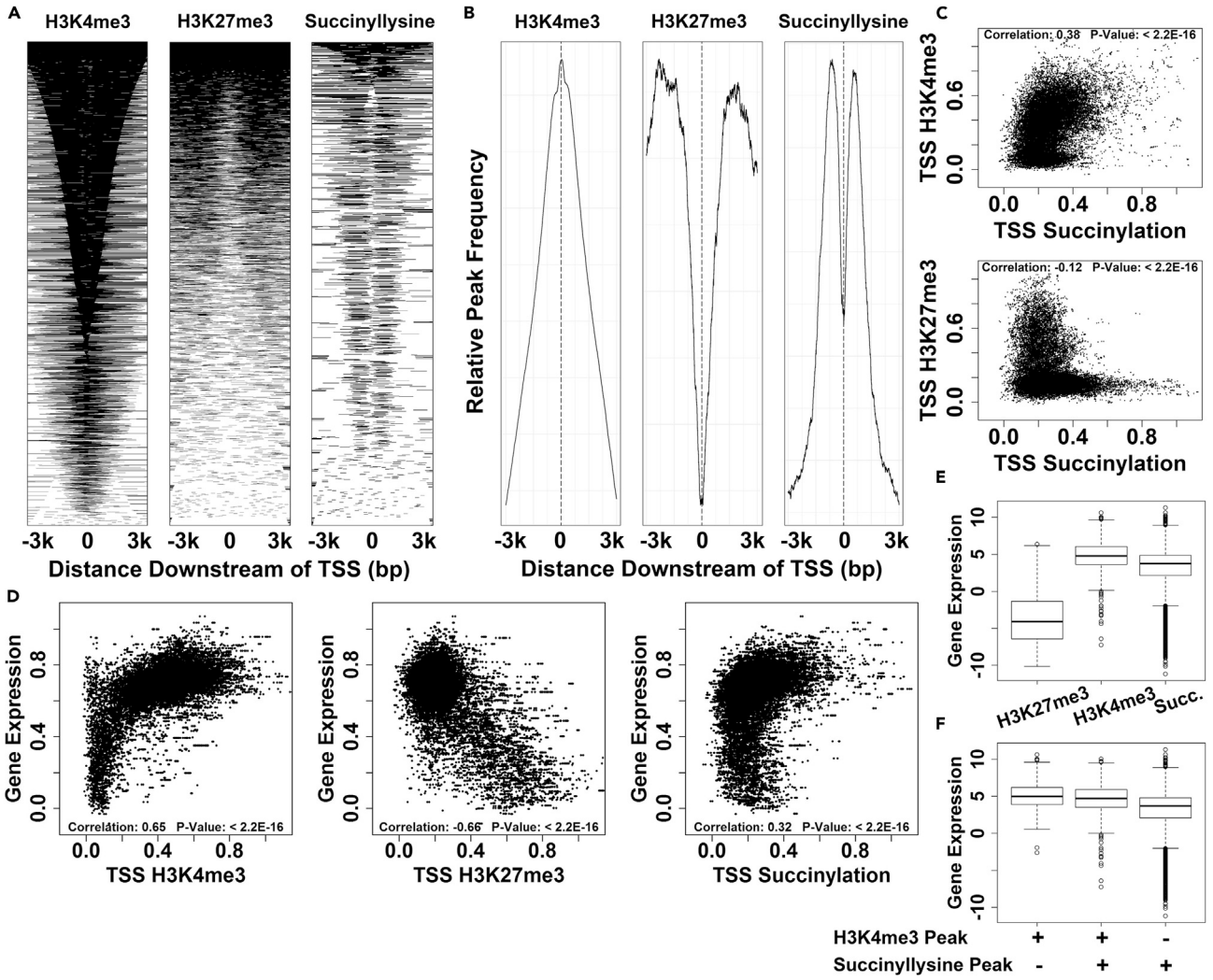

Figure 3. Chromatin Succinylation Exhibits Distinct Pattern of Localization Near Gene Promoters and Correlates with Gene Expression

(A) Plots of aligned probes showing chromatin mark enrichment over a 6-kbp window centered on the TSS. Individual lines on the plots correspond to specific TSS loci, with the shading of the plot representing the presence of ChIP-seq peaks. Genomic regions in the three plots are ordered independently according to the mean intensity.

(B) Probe trend plots covering a 6-kbp window centered on the TSS. Lines demonstrate relative peak frequency as a function of position, averaged across all annotated TSS.

(C) Analysis of correlation between succinyllysine signal intensity and intensities of known histone marks (H3K4me3 and H3K27me3) at TSS (4-kbp window centered on TSS).

(D) Analysis of correlation between chromatin ChIP-seq mark TSS abundance and gene expression (log_2-transformed fragments per kilobase million (FPKM) values, then scaled in range of 0–1).

(E) Analysis of expression in subsets of genes containing ChIP-seq peaks within 3 kbp of the TSS for H3K27me3, H3K4me3, or succinyllysine. y Axis shows log_2-transformed gene expression FPKM values.

(F) Detailed analysis of gene expression in subset of genes containing TSS-localizing ChIP-seq peaks for H3K4me3 and/or succinyllysine.

succinylation of nucleosome core particles with succinic anhydride enhances transcription, possibly through electrostatic effects (Piñeiro et al., 1992). The findings of these early studies ultimately support our *in vivo* work analyzing genome-wide patterns of succinylation in chromatin and assessing correlations with gene expression. When taken together, these data support a claim that chromatin succinylation in gene promoters is transcription activating. Unlike acetylation, which neutralizes potential favorable interactions between cationic lysine side chains and anionic DNA or histone sites, succinylation converts the cationic lysine side chain to an anion with much greater potential for electrostatic disruption. This possible electrostatic mechanism for promoting an active chromatin state remains to be explored.

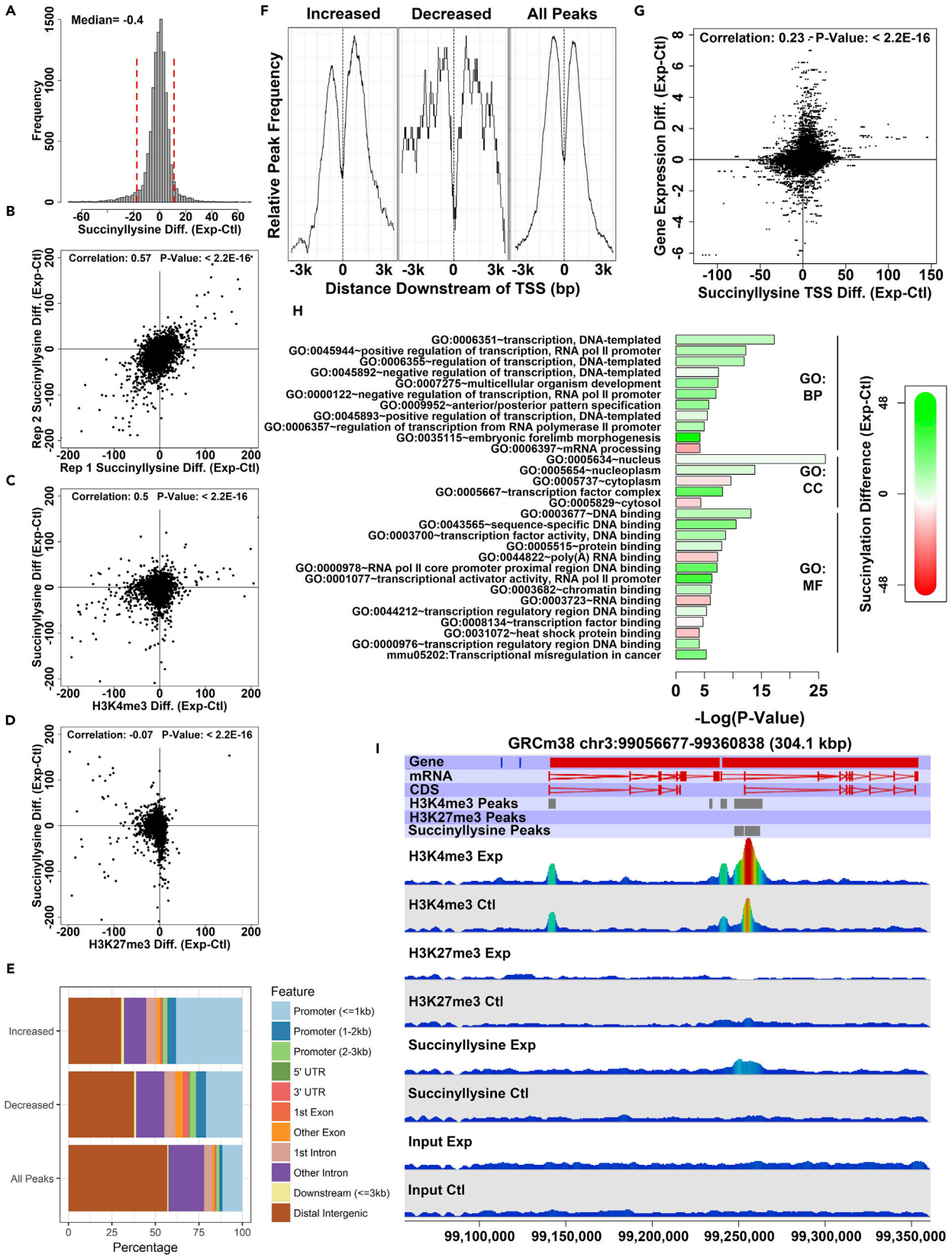
A
Median= -0.4
Frequency
Succinyllysine Diff. (Exp-Ctl)
B
Correlation: 0.57 P-Value: < 2.2E-16
Rep 2 Succinyllysine Diff. (Exp-Ctl)
Rep 1 Succinyllysine Diff. (Exp-Ctl)
C
Correlation: 0.5 P-Value: < 2.2E-16
Succinyllysine Diff (Exp-Ctl)
H3K4me3 Diff. (Exp-Ctl)
D
Correlation: -0.07 P-Value: < 2.2E-16
Succinyllysine Diff. (Exp-Ctl)
H3K27me3 Diff. (Exp-Ctl)
E
Increased
Decreased
All Peaks
Percentage
Feature
Promoter (<=1kb)
Promoter (1-2kb)
Promoter (2-3kb)
5' UTR
3' UTR
1st Exon
Other Exon
1st Intron
Other Intron
Downstream (<=3kb)
Distal Intergenic
F
Increased
Decreased
All Peaks
Relative Peak Frequency
Distance Downstream of TSS (bp)
G
Correlation: 0.23 P-Value: < 2.2E-16
Gene Expression Diff. (Exp-Ctl)
Succinyllysine TSS Diff. (Exp-Ctl)
H
GO:0006351~transcription, DNA-templated
GO:0045944~positive regulation of transcription, RNA pol II promoter
GO:0006355~regulation of transcription, DNA-templated
GO:0045892~negative regulation of transcription, DNA-templated
GO:0007275~multicellular organism development
GO:0000122~negative regulation of transcription, RNA pol II promoter
GO:0009952~anterior/posterior pattern specification
GO:0045893~positive regulation of transcription, DNA-templated
GO:0006357~regulation of transcription from RNA polymerase II promoter
GO:0035115~embryonic forelimb morphogenesis
GO:0006397~mRNA processing
GO:0005634~nucleus
GO:0005654~nucleoplasm
GO:0005737~cytoplasm
GO:0005667~transcription factor complex
GO:0005829~cytosol
GO:0003677~DNA binding
GO:0043565~sequence-specific DNA binding
GO:0003700~transcription factor activity, DNA binding
GO:0005515~protein binding
GO:0044822~poly(A) RNA binding
GO:0000978~RNA pol II core promoter proximal region DNA binding
GO:0001077~transcriptional activator activity, RNA pol II promoter
GO:0003682~chromatin binding
GO:0003723~RNA binding
GO:0044212~transcription regulatory region DNA binding
GO:0008134~transcription factor binding
GO:0031072~heat shock protein binding
GO:0000976~transcription regulatory region DNA binding
mmu05202:Transcriptional misregulation in cancer
GO: BP
GO: CC
GO: MF
Succinylation Difference (Exp-Ctl)
-Log(P-Value)
I
GRCm38 chr3:99056677-99360838 (304.1 kbp)
Gene
mRNA
CDS
H3K4me3 Peaks
H3K27me3 Peaks
Succinyllysine Peaks
H3K4me3 Exp
H3K4me3 Ctl
H3K27me3 Exp
H3K27me3 Ctl
Succinyllysine Exp
Succinyllysine Ctl
Input Exp
Input Ctl
99,100,000
99,150,000
99,200,000
99,250,000
99,300,000
99,350,000

Figure 4. SDH Loss Results in Reproducible Perturbation of Chromatin Succinylation that Preferentially Affects the Promoters of Genes Involved in Transcriptional Regulation

(A) Distribution of observed differences in succinylation peak integrated areas between experimental (SDHC loss) and control cell lines. Vertical red lines indicate the cutoff positions for 0.05 and 0.95 quantiles.

(B) Correlation analysis of observed succinylation peak integrated intensity differences (experimental minus control) between replicate experiments (see also Figure S3).

(C) Correlation analysis of changes (experimental minus control) in succinyllysine and H3K4me3 integrated intensities measured at the positions of succinyllysine ChIP-seq peaks.

(D) Correlation analysis of changes (experimental minus control) in succinyllysine and H3K27me3 integrated intensities measured at the positions of succinyllysine ChIP-seq peaks.

(E) Analysis of genomic feature localization for succinyllysine peaks showing dramatic integrated intensity differences resulting from SDHC loss. 0.05 and 0.95 quantiles, as shown in panel (A). x Axis indicates percentage of identified peaks mapping to a given feature type. See also Figure S3.

(F) Average profile plot showing TSS relative position for succinyllysine peaks showing dramatic integrated intensity differences resulting from SDHC loss. See also Figure S3.

(G) Analysis of correlation between promoter succinyllysine integrated intensity change and gene expression change [experimental minus control $\log_2$(FPKM)]; see also Figure S3.

(H) DAVID functional enrichment analysis of gene ontology impact for top 0.95 quantile of gene TSS (ranked according to absolute value of difference) affected by differential succinylation. x Axis value indicates degree of statistical significance for term enrichment relative to random gene set of the same size. Colors indicate mean succinyllysine difference (experimental minus control integrated TSS values) for differentially succinylated genes mapping to a given term (green, increased succinylation in experimental line; red, decreased succinylation in the experimental line).

(I) Representative genomic view of mouse chromosome 3 showing a succinyllysine peak dramatically affected by SDHC loss. Shown are genomic annotations for genes, mRNA, CDS, identified ChIP-seq peaks, and wiggle plot representations of mapped reads from the various ChIP-seq experiments; see also Figure S4.

To assess whether chromatin succinylation patterns merely reflect the H3K4me3 status of a given promoter, or whether chromatin succinylation encodes unique information, we next assessed gene expression as a function of mapped ChIP-seq peaks for the various immunoprecipitation experiments. Comparing gene expression with ChIP-seq peaks for H3K27me3, H4K4me3, and succinyllysine, we observe that genes whose promoter chromatin is enriched in H3K27me3 marks are poorly expressed, whereas genes whose promoter chromatin is enriched in H3K4me3 or succinyllysine marks are strongly expressed (Figure 3E). We further classified promoters as having H3K4me3 marks, succinyllysine marks, or both. This analysis showed that even for promoters enriched in succinyllysine marks without H3K4me3 marks, gene expression levels were among the highest in the cell (Figure 3F). This result suggests that chromatin succinylation represents a novel information-carrying mark of gene activation that is non-redundant with H3K4me3.

SDH Loss Perturbs Genome-wide Chromatin Succinylation

We next assessed how SDH loss affects genome-wide chromatin succinylation. Our previous analysis of bulk protein succinylation after SDH loss demonstrated increased protein succinylation, including several chromatin components (Figure 1J). This analysis did not reveal how the distribution of succinyllysine chromatin marks changes genome-wide upon SDH loss. We therefore mapped succinyllysine chromatin marks in SDH knockout and control cell lines. Interestingly, this analysis revealed a small net *decrease* in mapped read abundance at positions of succinyllysine peaks in the SDH knockout line relative to control, but with a particular subset of loci displaying dramatic perturbation (Figure 4A). This result was reproducible, as indicated by a high degree of correlation between the results of replicate experiments (Pearson correlation coefficient: 0.57; p value $< 2.2 \times 10^{-16}$; Figure 4B). Analysis of the correlation between succinyllysine change and changes in histone marks at succinyllysine peaks revealed that change in succinyllysine marks is positively correlated with perturbation of H3K4me3 (Figure 4C) and negatively correlated with H3K27me3 (Figure 4D) marks. An observed positive correlation between succinylation and H3K4me3 changes is particularly intriguing, given the potential for succinylation and methylation at a given histone lysine position to be mutually exclusive and competing PTMs.

SDH Loss Selectively Perturbs Chromatin Succinylation in Promoters

We assessed which genomic regions undergo the greatest change in chromatin succinylation upon SDH loss. For this analysis, we selected the top 0.05 and bottom 0.95 quantiles of ChIP-seq peaks, ranked by observed succinylation difference (SDH knockout minus control). Thus these peaks correspond to the subset of peaks that display extreme hypersuccinylation and hyposuccinylation, respectively, upon SDH loss. We mapped these highly affected peaks relative to the population of all chromatin succinyllysine peaks. Intriguingly, the alteration preferentially affects gene promoters (Figures 4E and 4F), with 45% of hypersuccinylated peaks and 30% of hyposuccinylated peaks mapping to promoters, compared with 15% of peaks

belonging to the parental distribution. The fact that succinylation change in chromatin following SDH loss is highly enriched in gene promoters over other types of genomic regions further underscores the potential transcriptional regulatory role of this mark. Subsequent analysis of the perturbation H3K4me3 and H3K27me3 marks upon SDH loss yielded the similar finding that epigenetic impacts are concentrated in promoter regions (Figures S3A–S3H and S4A–S4C). Although the mechanism remains unknown, the observation that TCA cycle dysfunction due to SDH loss has concerted effects on chromatin succinylation in gene promoters emphasizes the apparent regulatory specificity of this novel mark.

Chromatin Succinylation Changes upon SDH Loss Correlate with Gene Expression Changes

We assessed whether changes in promoter chromatin succinylation upon SDH loss correlate with induced alterations in gene expression. Our previous analysis of the correlation between promoter succinylation and gene expression in normal cells showed that succinylation is a feature of highly expressed genes (Figures 3D–3F). We therefore hypothesized that changes in chromatin succinylation upon SDH loss would directly correlate with observed gene expression changes. This hypothesis is indeed supported by the data (Spearman correlation coefficient: 0.23; p value $< 2.2 \times 10^{-16}$; Figure 4G). This result suggests that either perturbation of chromatin succinylation causes altered gene expression or that the succinylation status of specific genomic loci dynamically changes to reflect perturbed gene expression patterns. Under either model, this observation constitutes a quantifiable transcriptional phenotype that is correlated with alterations in genome-wide succinylation of gene promoters.

Changes in Chromatin Succinylation upon SDH Loss Selectively Affect Promoters of Genes Involved in Transcriptional Regulation

We assessed the extent to which chromatin succinylation plays a role in regulating the expression of genes controlling specific processes or pathways. We used the DAVID functional annotation database (Huang da et al., 2009) to perform functional annotation enrichment analysis on the top 0.05 quantile of differentially succinylated promoters for known gene ontologies, ranked according to the absolute value of succinylation change. The results (Figure 4H) reveal a genome-wide phenotype of selective hypersuccinylation impact on genes involved in transcriptional regulation and a specific hyposuccinylation effect upon genes involved in RNA processing. These trends provide strong evidence that chromatin succinylation cues specific transcriptional programs within cells. A representative genomic view displaying altered chromatin succinylation in the context of SDH loss is shown in Figure 4I.

Collectively, these observations support the hypothesis that chromatin succinylation is a link between the TCA cycle status and epigenetic transcriptional control. This result has implications both for normal cell growth and homeostasis, and for the mechanism of oncometabolites, such as succinate, that accumulate due to mutations affecting TCA cycle enzymes.

SDH Loss Results in a DNA Repair Defect Consistent with Chromatin Hypersuccinylation Effects

We next assessed whether SDH loss results in a DNA repair defect that is consistent with hypersuccinylation effects, similar to that observed in the context of SIRT7 depletion (Li et al., 2016). In the context of SIRT7 desuccinylase depletion, a defect in PARP1-dependent DNA repair becomes evident that is linked to failure in histone desuccinylation and chromatin compaction essential for repairing genotoxic damage. Upon genotoxic insult, SIRT7 −/− cells display abnormally elevated levels of gamma H2A.X, a marker for DNA damage. We therefore investigated whether hypersuccinylation of chromatin in the context of SDH phenocopies SIRT7 by similarly exhibiting a DNA repair defect. Strikingly, we observe that SDH loss results in heightened levels of DNA damage marker gamma H2A.X (phospho 139) (Figures 5A and 5B), consistent with a global DNA repair defect attributable to hypersuccinylation effects. Remarkably, this elevation in gamma H2A.X (phospho 139) occurs in the absence of an external genotoxic insult, suggesting that SDH loss results in a DNA repair defect that allows for accumulation of normal replication-induced errors to abnormally high levels. We additionally show that this intrinsic DNA repair defect predisposes SDH loss cells to be sensitive to genotoxic drugs such as gemcitabine (Figure 5C) and etoposide (Figure 5D), further validating the claim of a DNA repair defect in the setting of SDH loss. This enhanced sensitivity to genotoxic compounds such as these is particularly remarkable because these compounds mediate toxicity during DNA replication and SDH loss results in slowed population doubling time (Smestad et al., 2017). Collectively, these experiments suggest that chromatin hypersuccinylation may

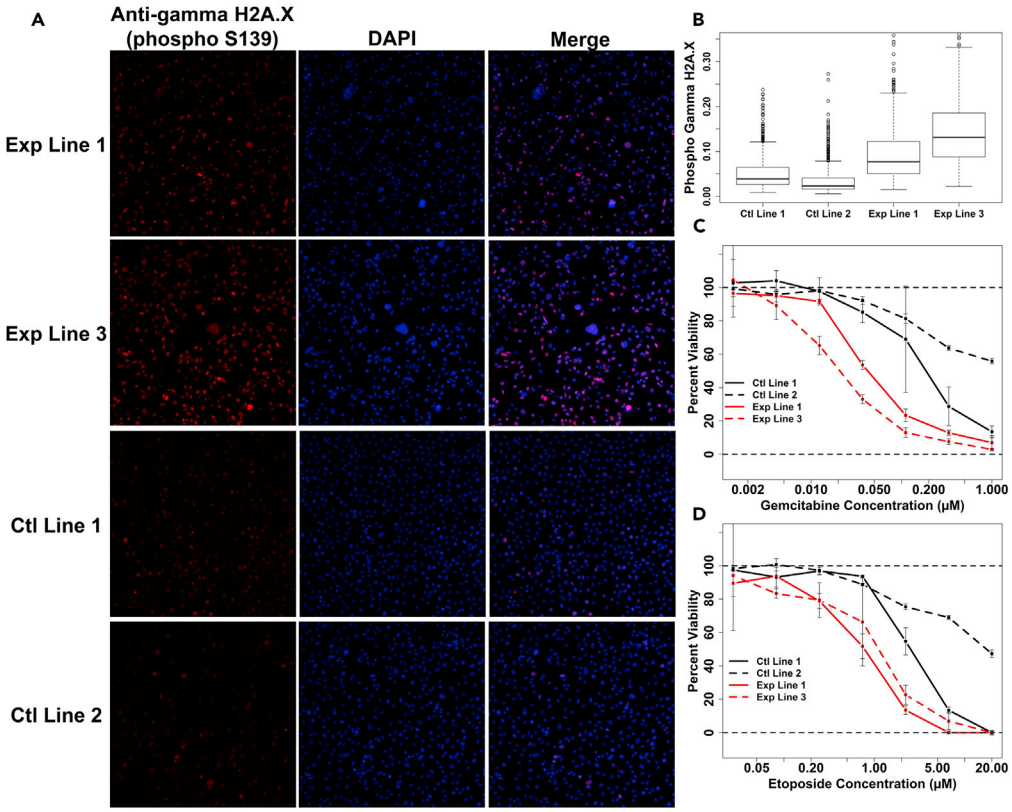

Figure 5. SDH Loss Results in a DNA Repair Defect Consistent with Chromatin Hypersuccinylation Effects

(A) Immunostaining for gamma H2A.X (phospho 139), with 4′,6-diamidino-2-phenylindole (DAPI) counterstain. Shown are representative images for two stable experimental (SDH loss) and control cell lines.

(B) Quantification of mean nuclear gamma H2A.X (phospho 139) immunostain intensity using automated image analysis.

(C) Analysis of differential cell line viability as a function of gemcitabine concentration. Viability quantification is in reference to untreated condition, with error bars corresponding to standard deviations from triplicate assay replicates.

(D) Analysis of differential cell line viability as a function of etoposide concentration. Viability quantification is in reference to untreated condition, with error bars corresponding to standard deviations from triplicate assay replicates.

generally impede DNA repair activities and form tantalizing conceptual links to recent work connecting SIRT7 desuccinylase activity with chromatin compaction essential for repair of genotoxic DNA damage.

DISCUSSION

This work demonstrates for the first time that an SDH loss TCA cycle defect relevant to several human malignancies results in increased concentrations of succinyl-CoA and bulk protein hypersuccinylation affecting multiple subcellular compartments. Hypersuccinylation affects both histone and non-histone nuclear proteins. We estimate that more than one-third of all nucleosomes contain lysine succinylation marks and that this fraction is increased in the context of SDH loss. By investigating the genomic localization of succinyllysine modifications in chromatin via ChIP-seq, we show that succinyllysine ChIP-seq peaks are enriched in gene promoters and identify a bimodal pattern of peak enrichment flanking transcription start sites genome-wide that is suggestive of a role in transcriptional regulation. We also directly test the correlation between succinyllysine ChIP signal and gene expression. We find that there is indeed a strong correlation between gene expression and succinylation near the transcription start site and further show that promoter succinylation is strongly predictive of high gene expression. We further assess how succinyllysine marks in chromatin are perturbed in the context of SDH loss TCA cycle defect and show that chromatin succinylation changes are concentrated in gene promoters relative to other genomic regions. We show that promoter succinylation changes induced by SDH loss are correlated with observed transcriptional responses genome-wide, further underscoring the fact that promoter chromatin succinylation and gene expression are correlated.

Beyond *in vivo* correlative studies, the next level of evidence needed to establish that histone succinylation activates transcription could come from an *in vitro* assay to test this hypothesis under tightly controlled conditions. Conveniently, such assays have already been reported (Piñeiro et al., 1992). These early experiments involved treating histone octamers with succinic anhydride, reconstituting with transcriptional templates, and measuring the effects of nucleosome succinylation on transcription. Remarkably, the authors found that succinylated nucleosomes have potent transcription-activating properties. These studies, performed years before it was appreciated that succinylation is a relevant histone lysine PTM that occurs in living cells, strongly support our *in vivo* work analyzing genome-wide patterns of succinylation in chromatin and assessing correlations with gene expression. When taken together, these data strongly support a claim that chromatin succinylation in gene promoters activates transcription. It remains to be determined if the basis for this effect is primarily electrostatic, or if a family of regulatory succinyllysine "reader" proteins are also involved.

Finally, we demonstrate that SDH loss results in a DNA repair defect that may be linked to chromatin hypersuccinylation effects. Previous work performed by Li et al. has demonstrated that depletion of SIRT7 desuccinylase results in histone hypersuccinylation and a resultant defect in DNA double-strand break repair (Li et al., 2016). We were intrigued that SDH loss, another cause of histone hypersuccinylation, appears to phenocopy the DNA repair defect observed upon SIRT7 depletion. It is highly remarkable that the two currently known genetic causes of histone hypersuccinylation both result in DNA repair defects. Whether these observed DNA repair defects are related by a common mechanism remains to be determined.

METHODS

All methods can be found in the accompanying Transparent Methods supplemental file.

SUPPLEMENTAL INFORMATION

Supplemental Information includes Transparent Methods, four figures, and three tables and can be found with this article online at https://doi.org/10.1016/j.isci.2018.03.012.

ACKNOWLEDGMENTS

This work was facilitated by the Mayo Clinic Metabolomics Resource Core Facility (NIH grant U24DK100469), the Mayo Clinic Medical Genome Facility Sequencing Core, the Mayo Clinic Epigenetics Development Laboratory, and the Mayo Clinic Research Computing Facility. Financial support for this work was from the Mayo Clinic; NIH grants R01CA166025 (L.J.M.), T32GM065841 (Mayo Clinic Medical Scientist Training Program), and F30CA220660 (J.S.); and generous support from the Paradifference Foundation (L.J.M.).

AUTHOR CONTRIBUTIONS

Conceptualization, L.J.M., J.S., and Y.C.; methodology, L.J.M., J.S., L.E., and Y.C.; validation, J.S. and L.E.; formal analysis, J.S., L.E., and Y.C.; investigation, J.S. and L.E.; resources, L.J.M. and J.S.; data curation, J.S.; writing: original draft, J.S. and L.E.; writing: review and editing, L.J.M., J.S., Y.C., and L.E.; visualization, J.S.; supervision, L.J.M. and Y.C.; project administration, L.J.M. and Y.C.; funding acquisition, L.J.M.

DECLARATION OF INTERESTS

The authors declare no competing interests.

Received: October 23, 2017
Revised: January 18, 2018
Accepted: February 20, 2018
Published: April 27, 2018

REFERENCES

Agaimy, A. (2016). Succinate dehydrogenase (SDH)-deficient renal cell carcinoma. Pathologe *37*, 144–152.

Astuti, D., Latif, F., Dallol, A., Dahia, P.L., Douglas, F., George, E., Sköldberg, F., Husebye, E.S., Eng, C., and Maher, E.R. (2001). Gene mutations in the succinate dehydrogenase subunit SDHB cause susceptibility to familial pheochromocytoma and to familial paraganglioma. Am. J. Hum. Genet. *69*, 49–54.

Baysal, B.E., Ferrell, R.E., Willett-Brozick, J.E., Lawrence, E.C., Myssiorek, D., Bosch, A., van der Mey, A., Taschner, P.E., Rubinstein, W.S., Myers, E.N., et al. (2000). Mutations in SDHD, a mitochondrial complex II gene, in hereditary paraganglioma. Science *287*, 848–851.

Chen, Y., Sprung, R., Tang, Y., Ball, H., Sangras, B., Kim, S.C., Falck, J.R., Peng, J., Gu, W., and

Zhao, Y. (2007). Lysine propionylation and butyrylation are novel post-translational modifications in histones. Mol. Cell. Proteomics *6*, 812–819.

Choudhary, C., Kumar, C., Gnad, F., Nielsen, M.L., Rehman, M., Walther, T.C., Olsen, J.V., and Mann, M. (2009). Lysine acetylation targets protein complexes and co-regulates major cellular functions. Science *325*, 834–840.

Dai, L., Peng, C., Montellier, E., Lu, Z., Chen, Y., Ishii, H., Debernardi, A., Buchou, T., Rousseaux, S., Jin, F.L., et al. (2014). Lysine 2-hydroxyisobutyrylation is a widely distributed active histone mark. Nat. Chem. Biol. *10*, 365–U373.

Du, J.T., Zhou, Y.Y., Su, X.Y., Yu, J.J., Khan, S., Jiang, H., Kim, J., Woo, J., Kim, J.H., Choi, B.H., et al. (2011). Sirt5 is a NAD-dependent protein lysine demalonylase and desuccinylase. Science *334*, 806–809.

Garrity, J., Gardner, J.G., Hawse, W., Wolberger, C., and Escalante-Semerena, J.C. (2007). N-Lysine propionylation controls the activity of propionyl-CoA synthetase. J. Biol. Chem. *282*, 30239–30245.

Gill, A.J., Lipton, L., Taylor, J., Benn, D.E., Richardson, A.L., Frydenberg, M., Shapiro, J., Clifton-Bligh, R.J., Chow, C.W., and Bogwitz, M. (2013). Germline SDHC mutation presenting as recurrent SDH deficient GIST and renal carcinoma. Pathology *45*, 689–691.

Huang da, W., Sherman, B.T., and Lempicki, R.A. (2009). Systematic and integrative analysis of large gene lists using DAVID bioinformatics resources. Nat. Protoc. *4*, 44–57.

Ito, K., Barnes, P.J., and Adcock, I.M. (2000). Glucocorticoid receptor recruitment of histone deacetylase 2 inhibits interleukin-1 beta-induced histone H4 acetylation on lysines 8 and 12. Mol. Cell. Biol. *20*, 6891–6903.

Leemhuis, H., Packman, L.C., Nightingale, K.P., and Hollfelder, F. (2008). The human histone acetyltransferase P/CAF is a promiscuous histone propionyltransferase. Chembiochem *9*, 499–503.

Li, L., Shi, L., Yang, S., Yan, R., Zhang, D., Yang, J., He, L., Li, W., Yi, X., Sun, L., et al. (2016). SIRT7 is a histone desuccinylase that functionally links to chromatin compaction and genome stability. Nat. Commun. *7*, 12235.

McManus, K.J., and Hendzel, M.J. (2000). Specificity determination of CREB binding protein's (CBP) acetyltransferase activity for various histone lysine residues. Mol. Biol. Cell *11*, 307a.

Michishita, E., McCord, R.A., Berber, E., Kioi, M., Padilla-Nash, H., Damian, M., Cheung, P., Kusumoto, R., Kawahara, T.L., Barrett, J.C., et al. (2008). SIRT6 is a histone H3 lysine 9 deacetylase that modulates telomeric chromatin. Nature *452*, 492–496.

Nannini, M., Astolfi, A., Urbini, M., Indio, V., Santini, D., Heinrich, M.C., Corless, C.L., Ceccarelli, C., Saponara, M., Mandrioli, A., et al. (2014). Integrated genomic study of quadruple-WT GIST (KIT/PDGFRA/SDH/RAS pathway wild-type GIST). BMC Cancer *14*, 685.

Ni, Y., Seballos, S., Ganapathi, S., Gurin, D., Fletcher, B., Ngeow, J., Nagy, R., Kloos, R.T., Ringel, M.D., LaFramboise, T., et al. (2015). Germline and somatic SDHx alterations in apparently sporadic differentiated thyroid cancer. Endocr. Relat. Cancer *22*, 121–130.

Niemann, S., and Müller, U. (2000). Mutations in SDHC cause autosomal dominant paraganglioma, type 3. Nat. Genet. *26*, 268–270.

Olsen, J.V., Vermeulen, M., Santamaria, A., Kumar, C., Miller, M.L., Jensen, L.J., Gnad, F., Cox, J., Jensen, T.S., Nigg, E.A., et al. (2010). Quantitative phosphoproteomics reveals widespread full phosphorylation site occupancy during mitosis. Sci. Signal. *3*, ra3.

Pantaleo, M.A., Nannini, M., Corless, C.L., and Heinrich, M.C. (2015). Quadruple wild-type (WT) GIST: defining the subset of GIST that lacks abnormalities of KIT, PDGFRA, SDH, or RAS signaling pathways. Cancer Med. *4*, 101–103.

Park, J., Chen, Y., Tishkoff, D.X., Peng, C., Tan, M., Dai, L., Xie, Z., Zhang, Y., Zwaans, B.M., Skinner, M.E., et al. (2013). SIRT5-mediated lysine desuccinylation impacts diverse metabolic pathways. Mol. Cell *50*, 919–930.

Piñeiro, M., Hernández, F., and Palacián, E. (1992). Succinylation of histone amino-groups facilitates transcription of nucleosomal cores. Biochim. Biophys. Acta *1129*, 183–187.

Rardin, M.J., He, W., Nishida, Y., Newman, J.C., Carrico, C., Danielson, S.R., Guo, A., Gut, P., Sahu, A.K., Li, B., et al. (2013). SIRT5 regulates the mitochondrial lysine succinylome and metabolic networks. Cell Metab. *18*, 920–933.

Ravindra, K.C., Selvi, B.R., Arif, M., Reddy, B.A.A., Thanuja, G.R., Agrawal, S., Pradhan, S.K., Nagashayana, N., Dasgupta, D., and Kundu, T.K. (2009). Inhibition of lysine acetyltransferase KAT3B/p300 activity by a naturally occurring hydroxynaphthoquinone, plumbagin. J. Biol. Chem. *284*, 24453–24464.

Sadhukhan, S., Liu, X.J., Ryu, D., Nelson, O.D., Stupinski, J.A., Li, Z., Chen, W., Zhang, S., Weiss, R.S., Locasale, J.W., et al. (2016). Metabolomics-assisted proteomics identifies succinylation and SIRT5 as important regulators of cardiac function. Proc. Natl. Acad. Sci. USA *113*, 4320–4325.

Simithy, J., Sidoli, S., Yuan, Z.F., Coradin, M., Bhanu, N.V., Marchione, D.M., Klein, B.J., Bazilevsky, G.A., McCullough, C.E., Magin, R.S., et al. (2017). Characterization of histone acylations links chromatin modifications with metabolism. Nat. Commun. *8*, 1141.

Smestad, J., Hamidi, O., Wang, L., Holte, M.N., Khazal, F.A., Erber, L., Chen, Y., and Maher, L.J., 3rd (2017). Characterization and metabolic synthetic lethal testing in a new model of SDH-loss familial pheochromocytoma and paraganglioma. Oncotarget *9*, 6109–6127.

Tafrova, J.I., and Tafrov, S.T. (2014). Human histone acetyltransferase 1 (Hat1) acetylates lysine 5 of histone H2A in vivo. Mol. Cell. Biochem. *392*, 259–272.

Tan, M., Luo, H., Lee, S., Jin, F., Yang, J.S., Montellier, E., Buchou, T., Cheng, Z., Rousseaux, S., Rajagopal, N., et al. (2011). Identification of 67 histone marks and histone lysine crotonylation as a new type of histone modification. Cell *146*, 1016–1028.

Tan, M.J., Peng, C., Anderson, K.A., Chhoy, P., Xie, Z., Dai, L., Park, J., Chen, Y., Huang, H., Zhang, Y., et al. (2014). Lysine glutarylation is a protein posttranslational modification regulated by SIRT5. Cell Metab. *19*, 605–617.

Thul, P.J., Åkesson, L., Wiking, M., Mahdessian, D., Geladaki, A., Ait Blal, H., Alm, T., Asplund, A., Bjork, L., Breckels, L.M., et al. (2017). A subcellular map of the human proteome. Science *356*, eaal3321.

Wagner, G.R., Bhatt, D.P., O'Connell, T.M., Thompson, J.W., Dubois, L.G., Backos, D.S., Yang, H., Mitchell, G.A., Ilkayeva, O.R., Stevens, R.D., et al. (2017). A class of reactive Acyl-CoA species reveals the non-enzymatic origins of protein acylation. Cell Metab. *25*, 823–837.e8.

Wang, H., Chen, Y., and Wu, G. (2016). SDHB deficiency promotes TGFβ-mediated invasion and metastasis of colorectal cancer through transcriptional repression complex SNAIL1-SMAD3/4. Transl. Oncol. *9*, 512–520.

Warrener, R., Chia, K., Warren, W.D., Brooks, K., and Gabrielli, B. (2010). Inhibition of histone deacetylase 3 produces mitotic defects independent of alterations in histone H3 lysine 9 acetylation and methylation. Mol. Pharmacol. *78*, 384–393.

Xie, Z., Dai, J., Dai, L., Tan, M., Cheng, Z., Wu, Y., Boeke, J.D., and Zhao, Y. (2012). Lysine succinylation and lysine malonylation in histones. Mol. Cell. Proteomics *11*, 100–107.

Xie, Z., Zhang, D., Chung, D., Tang, Z., Huang, H., Dai, L., Qi, S., Li, J., Colak, G., Chen, Y., et al. (2016). Metabolic regulation of gene expression by histone lysine beta-hydroxybutyrylation. Mol. Cell *62*, 194–206.

Xiong, B., Lu, S.A., and Gerton, J.L. (2010). Hos1 is a lysine deacetylase for the Smc3 subunit of cohesin. Curr. Biol. *20*, 1660–1665.

Yang, Y.Y., Grammel, M., and Hang, H.C. (2011). Identification of lysine acetyltransferase p300 substrates using 4-pentynoyl-coenzyme A and bioorthogonal proteomics. Bioorg. Med. Chem. Lett. *21*, 4976–4979.

Zhang, W., Bone, J.R., Edmondson, D.G., Turner, B.M., and Roth, S.Y. (1998). Essential and redundant functions of histone acetylation revealed by mutation of target lysines and loss of the Gcn5p acetyltransferase. EMBO J. *17*, 3155–3167.

Zhang, Z., Tan, M., Xie, Z., Dai, L., Chen, Y., and Zhao, Y. (2011). Identification of lysine succinylation as a new post-translational modification. Nat. Chem. Biol. *7*, 58–63.

ISCI, Volume *2*

Supplemental Information

Chromatin Succinylation Correlates with Active Gene Expression and Is Perturbed by Defective TCA Cycle Metabolism

John Smestad, Luke Erber, Yue Chen, and L. James Maher III

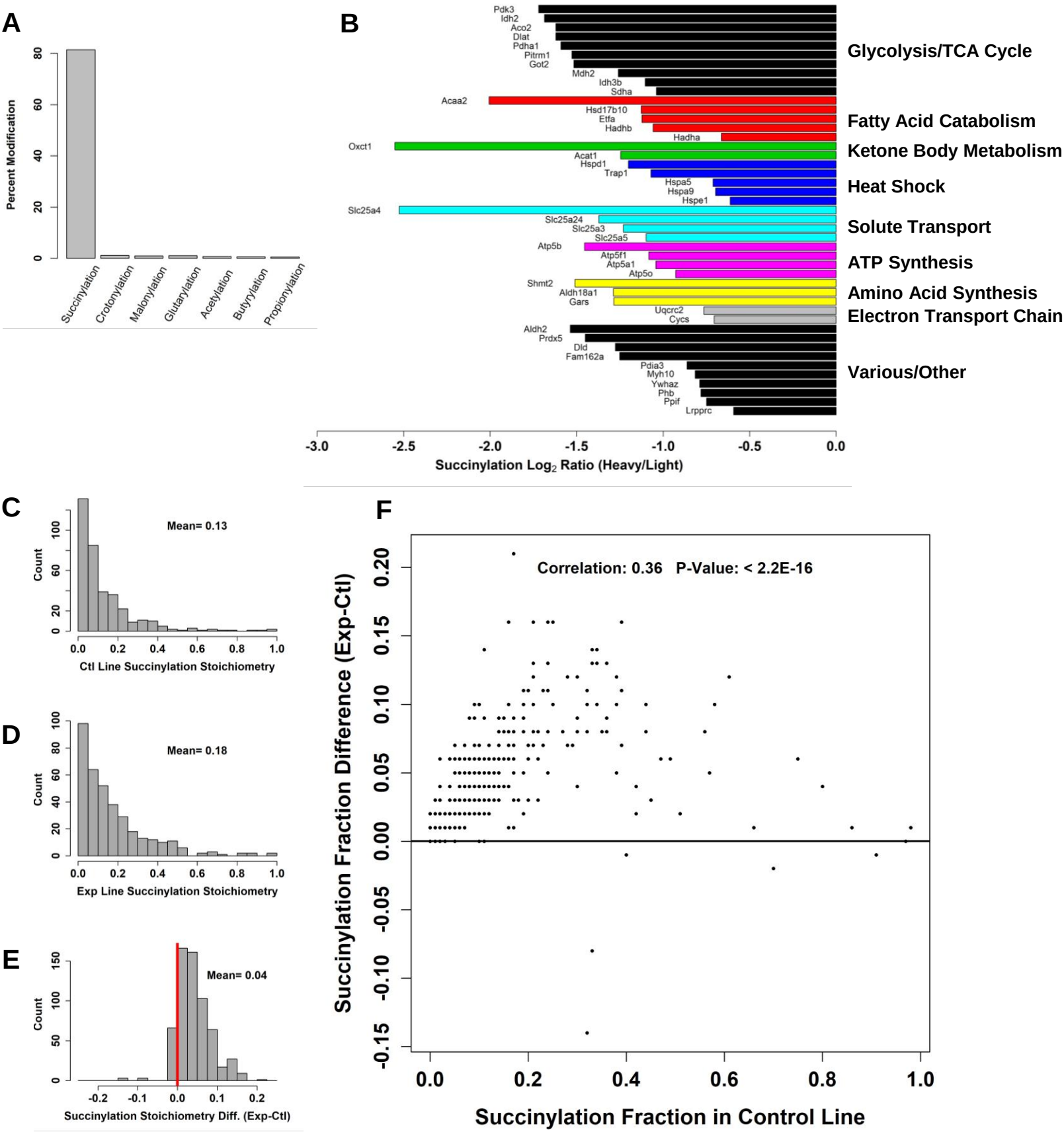

Figure S1. Related to Figure 1. Additional analysis of protein succinylation changes. A) Analysis of acylation modification prevalence in proteomic dataset following PTM-401 antibody pull-down. B) Relative succinylation changes for mitochondrial proteins identified as being differentially-succinylated in the context of SDHC loss, grouped according to functional role, supportive of Figure 1. C) Histogram showing distribution of succinylation stoichiometries in control cell line data set (N=364 succinylated sites quantified). D) Histogram showing distribution of succinylation stoichiometries in experimental cell line data set (N=364 succinylated sites quantified). E) Difference between succinylation stoichiometries identified in experimental and control cell line datasets. F) Analysis of correlation between succinylation stoichiometry difference (Exp-Ctl) and succinylation stoichiometry in control cell line.

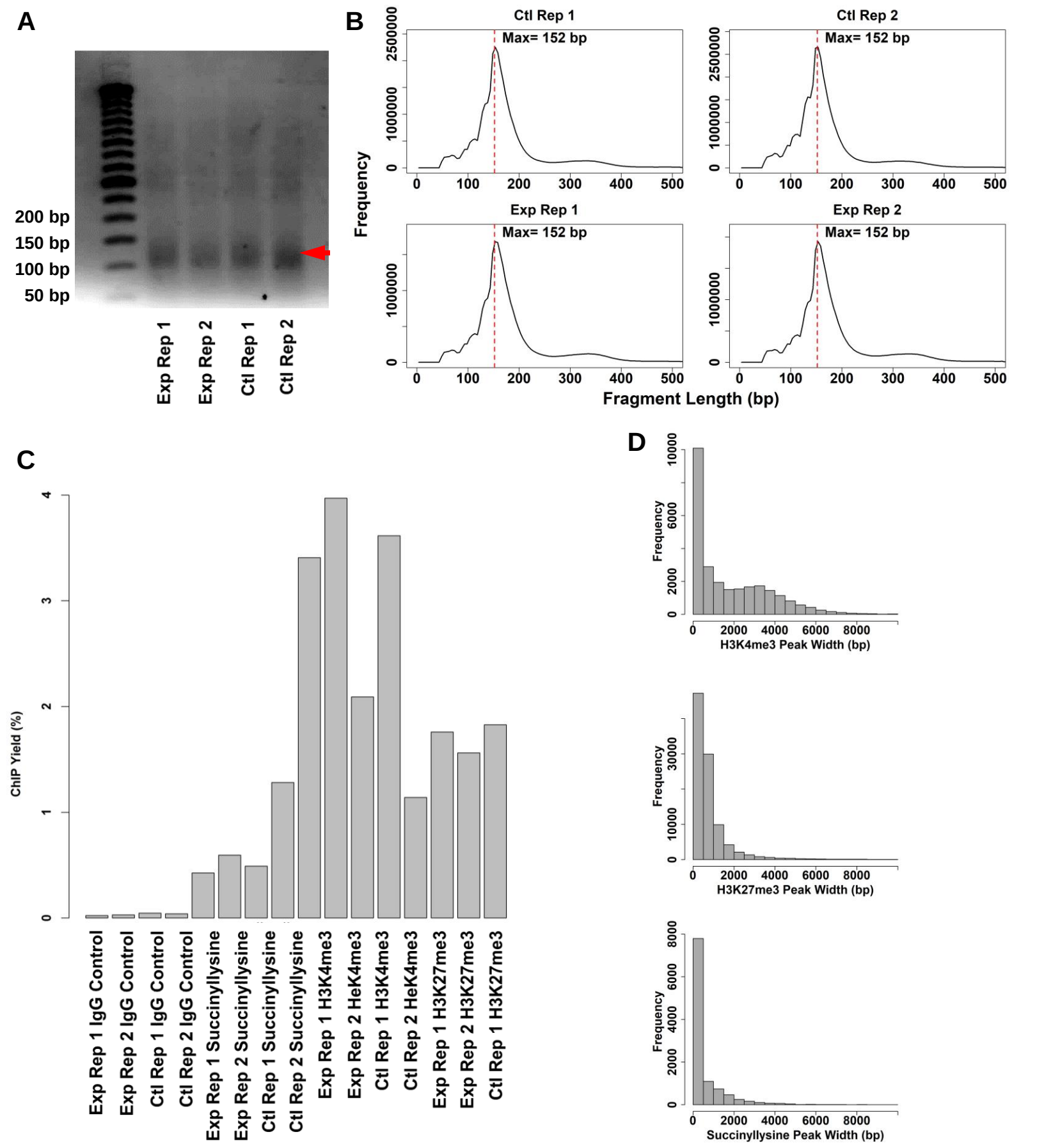

Figure S2. Related to Figure 2. Supplemental analysis of ChIP-seq experiment technical performance. A) Input chromatin size distribution assessed by gel electrophoresis (2% agarose gel; visualized with ethidium bromide) following cell lysis, MNase digestion, and sonication. Red arrow indicates position of highest band intensity. B) Paired end mapped fragment length quantified from ChIP-seq experiments. C) Quantified ChIP yields from pull-downs with anti-H3K4me3, anti-H3k27me3, and anti-succinyllysine antibodies. D) Widths of ChIP-seq peaks called via the MACS peak calling algorithm for H3K4me3, H3k27me3, and succinyllysine.

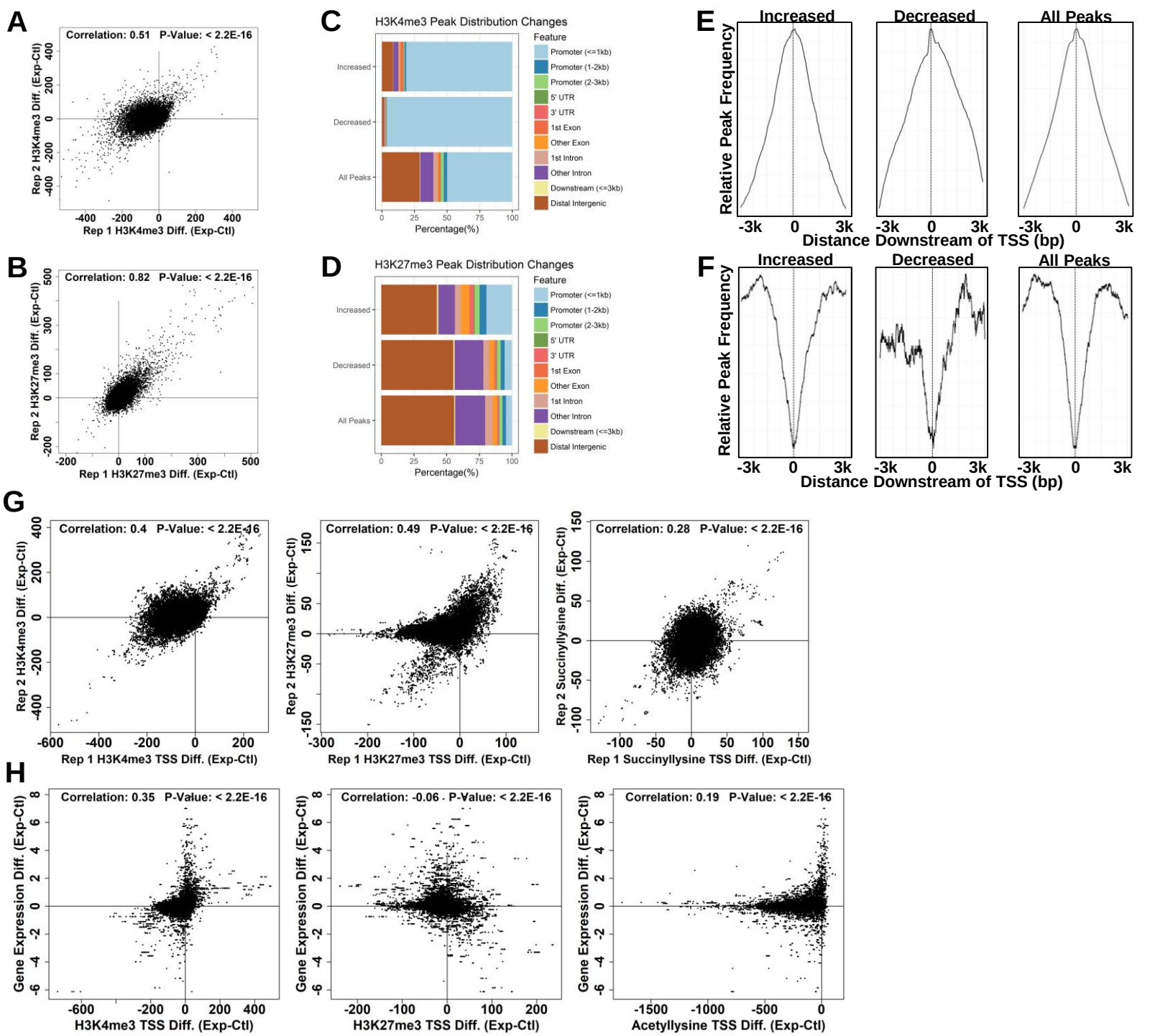

Figure S3. Related to Figure 4. Additional analysis of genome-wide H3K4me3 and H3K27me3 ChIP-peak intensity change patterns in response to SDHC loss and correlations with transcriptional effects. A) Correlation analysis of observed H3K4me3 peak integrated intensity differences (experimental minus control) between replicate experiments. B) Correlation analysis of observed H3K27me3 peak integrated intensity differences (experimental minus control) between replicate experiments. C) Analysis of genomic feature localization for H3K4me3 peaks showing dramatic integrated intensity differences resulting from SDHC loss. (0.05 and 0.95 quantiles, as shown in panel A). X-axis indicates percentage of identified peaks mapping to a given feature type. D) Analysis of genomic feature localization for H3K27me3 peaks showing dramatic integrated intensity differences resulting from SDHC loss. (0.05 and 0.95 quantiles, as shown in panel A). X-axis indicates percentage of identified peaks mapping to a given feature type. E) Average profile plot showing TSS relative position for H3K4me3 peaks showing dramatic integrated intensity differences resulting from SDHC loss. F) Average profile plot showing TSS relative position for H3K27me3 peaks showing dramatic integrated intensity differences resulting from SDHC loss. G) ChIP-seq difference correlations measured at TSS between biological replicate experiments, with each axis corresponding to differences between experimental and control lines. H) Correlations between changes in chromatin marks at TSS and changes in gene expression.

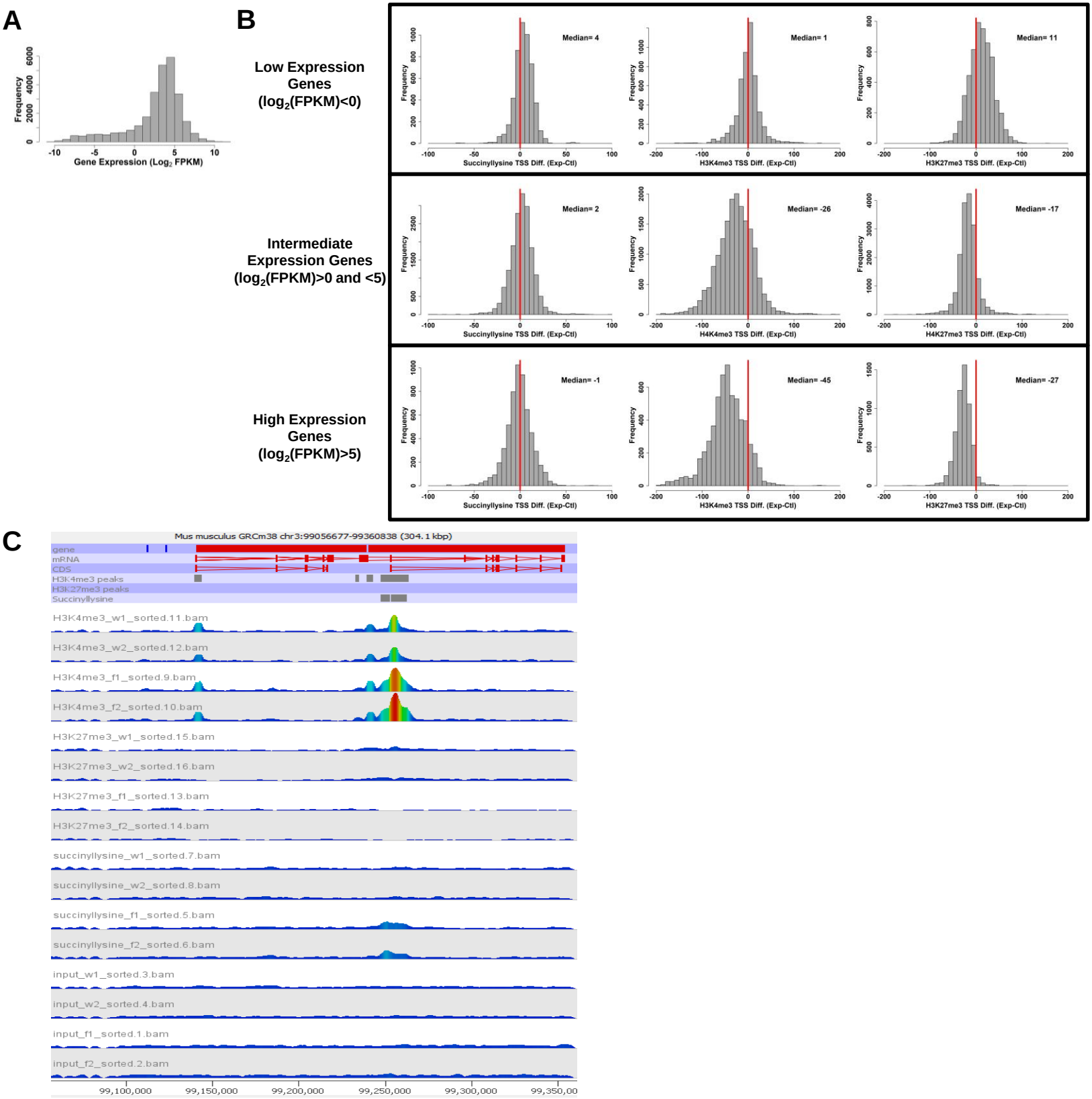

Figure S4. Related to Figure 4. Supplemental analysis of patterns of succinylation, H3K4me3, and H3K27me3 change at TSS in response to SDHC loss. A) Histogram showing distribution of gene expression values in control cell line. Gene expression is presented as $\log_2$-transformed FPKM values. B) Histograms showing distributions of succinyllysine, H3K4me3, and H3K27me3 changes (experimental minus control integrated intensities) measured at TSS, separated according to gene expression value in control cell line. Median values for distributions are indicated on plots. C) Representative genomic view of mouse chromosome 3 showing a succinyllysine peak dramatically affected by SDHC loss. Shown are genomic annotations for genes, mRNAs, CDS, identified ChIP-seq peaks, and wiggle plot representations of mapped reads from the various ChIP-seq experiments. Shown are two biological replicates for each experiment type.

Transparent Methods

CONTACT FOR REAGENT AND RESOURCE SHARING

Further information and requests for resources and reagents should be directed to and will be fulfilled by the lead contact, L.J. Maher (maher@mayo.edu).

EXPERIMENTAL MODEL AND SUBJECT DETAILS

Immortalized mouse embryonic fibroblast cell lines

The cell lines used in this study has been described previously (Smestad et al., 2017). Briefly, R26M2rtTA/+;TetOcre;Sdhcfl/fl (experimental) and R26M2rtTA/+;TetOcre;Sdhc fl/+ (control) mouse embryonic fibroblast lines (MEFs) were derived by crossing Sdhcfl/fl;R26M2rtTA/M2rtT mice with Sdhcfl/wt;TetOcre mice, harvesting and homogenizing day 13 embryos, and culturing in DMEM containing penicillin/streptomycin antibiotics (0.5 mg/mL), non-essential amino acids (100 micromolar each of glycine, alanine, asparagine, aspartic acid, glutamic acid, proline, and serine), sodium pyruvate (1 mM), and HEPES buffer (10 mM) at 21% O_2 and 5% CO_2. Cells were grown to superconfluence, split and transduced with SV-40 lentivirus, and then iteratively split at high dilution to yield purified populations of immortalized mouse embryonic fibroblasts (iMEFs). Sex of both experimental and control iMEF cell lines was determined to be female through analysis of sex chromosome aligned reads from ChIP-seq experiments. For routine cell culture subsequent to line derivation, cells were grown in DMEM containing 10% FBS, penicillin/streptomycin antibiotics (0.5 mg/mL each) at 21% O_2 and 5% CO_2.

METHOD DETAILS

TCA cycle metabolomics

For TCA cycle metabolomic studies, experimental (R26M2rtTA/+;TetOcre;Sdhcfl/fl) and control (R26M2rtTA/+;TetOcre;Sdhcfl/wt) iMEF cells were grown in DMEM containing 10% FBS, penicillin/streptomycin antibiotics (0.5 mg/mL each) at 21% O_2 and 5% CO_2. To induce *Sdhc* gene rearrangement, doxycycline hyclate (Sigma Aldrich cat# D9891-25G) was added to media to final concentration of 1 microgram/mL. Cells were grown for 16 d under these conditions, harvested by scraping, washed 3X with PBS, and then submitted to the Mayo Clinic Metabolomics Resource Core for targeted TCA cycle metabolomics studies. For both experimental and control cell lines, these experiments were performed in triplicate. Measured metabolite levels were normalized to total intracellular protein.

For succinyl-CoA measurements, cells were grown as describe above, and the same number of experimental and control cells harvested, washed 2X with PBS, homogenized in 10% trichloroacetic acid (TCA), and immobilized on a C18 SepPak cartridge pre-conditioned with methanol and water. Immobilized metabolites were washed 3X with 2 mL water and then eluted with 2X 0.75 mL methanol. Methanol eluents were diluted to 20% total volume and then lyophilized. Dried eluents were then reconstituted in 100 microliters 0.1M NaOH and CoA esters hydrolyzed by incubation at 40 degrees Celsius for 1 hour. Solutions were neutralized by the addition of 10 microliters of 1M HCl, and then the pH of the solutions stabilized by the addition of 20 microliters of 1 M tris-HCl (pH 7.5). Succinate concentrations in samples were then

quantified in triplicate using the BioVision succinate colorimetric assay kit (BioVision cat # K649).

Succinyllysine immunostaining

Following induction of SDHC loss, experimental and control cells were plated into 96 well plates at a density of 25,000 cells per well in 100 microliters of DMEM media containing 10% FBS, penicillin/streptomycin antibiotics (0.5 mg/mL each), 1 mM pyruvate, 1X MEM NEAA, and 10 mM HEPES buffer (pH7.2-7.5) at 21% O_2 and 5% CO_2. 6 hours after plating, media was aspirated and cells were washed with 100 microliters of PBS, fixed with 100 microliters of 3.7% formaldehyde in PBS for 20 minutes at room temperature, and permeabilized with 100 microliters of 0.1% Triton X-100 in PBS for 15 minutes at room temperature. Cells were then incubated with anti-succinyllysine (PTM Biolabs cat# PTM-401) primary antibody diluted 1:200 into PBS containing 10% FBS for 1 hour at room temperature with gentle shaking. Cells were then washed 5X with 100 microliters of PBS, and then incubated for 30 minutes at room temperature with goat anti-rabbit IgG (H+L) Alexa Fluor 488 (Invitrogen cat# A32731) diluted 1:500 into PBS containing 10% FBS. Cells were then washed 5X with 100 microliters PBS, and then counterstained with DAPI prior to imaging on a Zeiss LSM 780 confocal microscope. For each visual field, an autofocus routine was implemented to capture the plane with the highest DAPI staining intensity. Automated image analysis was then employed to quantify compartment-specific succinylation patterns, as previously described (Carpenter et al., 2006).

Gamma H2A.X phospho 139 immunostaining

Immunostaining for gamma H2A.X phospho 139 was performed using the same general protocol as described for succinyllysine immunostaining (see above), with a mouse monoclonal primary antibody against gamma H2A.X phospho 139 (Abcam cat# ab26350) used at 1:500 dilution, and a goat anti-mouse IgG (H+L) Alexa Fluor 594-conjugated secondary antibody (Invitrogen cat# A11032) used at 1:500 dilution.

Genotoxic drug studies

Cells from two stable SDH loss (experimental) and hemizygous control iMEF lines were plated into wells of a 96 well plate at concentration of 25,000 cells per 100 microliters of DMEM media (without phenol red) containing 10% FBS, penicillin/streptomycin antibiotics (0.5 mg/mL each), 1 mM pyruvate, 1X MEM NEAA, and 10 mM HEPES buffer (pH7.2-7.5) at 21% O_2 and 5% CO_2. Cells were allowed to attach to plate for 12 hours, and then 1 microliter of solutions containing genotoxic drugs (or vehicle control) were added to wells. Dilutions of etoposide were made into DMSO, with final concentrations of drugs ranging from 20 μM to 27 nM. Dilutions of gemcitabine were made into sterile water, with final concentrations ranging from 1 μM to 1 nM. After addition of drugs to cells, the plates were thoroughly mixed and incubated at 37 degrees with 21% O_2 and 5% CO_2 for 48 hours. 10 μL Alamar Blue (Thermo Fisher) cell viability reagent was added to each well. Plates were incubated for 36 h prior to taking absorbance measurements at 570 and 600 nm.

SILAC labeling

SILAC labeling of cells using heavy arginine and lysine was performed using with a commercially-available kit purchased through Thermo Fisher (cat # 89983 and cat #

88210). Reconstitution of arginine and lysine into media was performed according to product specifications. *Sdhc* fl/fl (experimental) cells were grown in "light" SILAC media and *Sdhc* fl/wt cells were grown in "heavy" media in T75 flasks at 37°C with 5% CO_2 and 21% O_2. For each cell line, labeling was performed in duplicate in separate flasks. On the same day as cells were started in SILAC media, doxycycline (2 micromolar) was added to the media to induce *Sdhc* gene rearrangement. Media was changed and cells passaged every 2-3 d to maintain between 20-90% confluence for a total of 16 d. On day 12 post induction with doxycycline, cells were expanded into T150 flasks. On day 16 post induction with doxycycline, media was aspirated, and adherent cells washed twice with 10 mL cold PBS. Cells were then harvested by scraping, transferred into 1.7 mL microcentrifuge tubes, subjected to centrifugation for 5 min at 500 X g, supernatant aspirated, and wet cell pellets flash frozen and stored in -80°.

Cell lysis and protein digestion

Following SILAC labeling, both experimental and control cells were homogenized in the urea lysis buffer (9M urea in PBS [pH 7.2] with 25 mM sodium butyrate, 50 mM nicotinamide and HALT protease inhibitor cocktail (Thermo Fisher)) followed by protein reduction and alkylation as previously described (Zhou et al., 2016). An equal amount of proteins from heavy and light labeled cells were mixed. The combined lysate was diluted six-fold in 1X PBS and proteins were digested with trypsin (1:50 enzyme to substrate ratio, w/w; Promega) at room temperature for overnight. A second tryptic digestion was performed (1:100 enzyme to substrate ratio, w/w) for 3 h to ensure complete digestion. Peptides were desalted with Sep-pack C18 cartridge (Waters) following the manufacturer’s instructions prior to enrichment.

Enrichment of lysine succinylated peptides

Succinylated peptides were enriched following the procedure as previously described (Park et al., 2013). Briefly, peptides were incubated with the agarose beads conjugated with the pan-anti succinyllysine antibody (PTM Biolabs) at 4 °C overnight. Following incubation, the beads were washed with NETN buffer (50 mM Tris HCl [pH 8.0], 100 mM NaCl, 1 mM EDTA, 0.5% NP40) and ETN buffer (50 mM Tris HCl [pH 8.0], 100 mM NaCl, 1 mM EDTA) sequentially. Peptides were eluted with 0.1% TFA and dried in a Speed-Vac device (Thermo Fisher) prior to desalting and fractionation. A small aliquot of peptides retained prior to the enrichment was processed directly for SCX fractionation and LCMS as described below for total protein quantification.

SCX fractionation

Peptides were desalted and fractionated with SCX using Empore membranes (3M) using a previously described method (Rappsilber et al., 2007). Briefly, peptides were loaded onto a Stage-tip containing Empore Cation Exchange-SR membranes (3M). The peptides were washed with 0.1% formic acid and then sequentially eluted with buffers consisting of 20% acetonitrile (v/v), 0.1% formic acid (v/v), and NH_4OAc with respective concentrations of 50, 75, 125, 200, 300, 500 mM. Subsequently, peptides from each fraction were desalted with C18 Stage-tips and dried with the Speed-Vac (Thermo Fisher).

LC-MS/MS measurement

Peptide samples were resuspended with HPLC buffer A (0.1% formic acid in water, v/v) and loaded onto an C18 column packed in-house (15 cm × 75 µm, ReproSil-

Pur Basic C18, 2.5 µm, Dr. Maisch GmbH). The samples were separated and analyzed with a Proxeon Easy nLC 1000 Nano-UPLC system connected online to an Orbitrap Fusion mass spectrometer (Thermo Fisher). Peptides were eluted with a 56-min gradient of 5-30% of HPLC buffer B (0.1% formic acid in acetonitrile, v/v) at a flow rate of 200 nL/min. The Fusion Orbitrap was operated in a data-dependent mode, prioritizing the most intense precursor ions. Full mass spectra were acquired with a resolution of 60,000 at m/z 300-1500 and MS/MS spectra were acquired using collision dissociation (CID) with 35% collision energy for detection in the ion trap.

Cell fixation

Experimental and control cell lines were grown for 16 d post induction with doxycycline, as described for the TCA metabolomics experiments. Cells (~10E6 count) were harvested by trypsinization and fixed with formaldehyde (methanol-free, Pierce cat# 28906) at 1% final concentration at room temperature for 10 min with gentle agitation. The fixation reaction was quenched by the addition of 0.5 mL 2.5 M glycine per 10 mL total volume, and incubated with mixing at room temperature for 5 min. Cells were then pelleted by centrifugation (3000 X g for 5 min), washed with 3 mL of cold TBS (50 mM Tris-HCl pH7.4, 150 mM NaCl) and counted with a hemacytometer, subjected to centrifugation again (3000 X g for 5 min at 4°C), and then wet cell pellets were stored at -80°C until use in ChIP experiments.

Chromatin preparation

Cell pellets were resuspended in 3 mL cell lysis buffer (10 mM Tris-HCl, pH 7.5, 10 mM NaCl, 0.5% IGEPAL) with gentle vortex agitation, and then incubated on ice for

15 min. Cells were pelleted by centrifugation (3000 X g for 5 min at 4°C) and the supernatant discarded. The pellet was resuspended in 450 microliters of MNase digestion buffer (20 mM Tris-HCl, pH 7.5, 15 mM NaCl, 60 mM KCl, 1 mM $CaCl_2$), subjected to centrifugation (12,000 rpm for 3 min), and supernatant discarded. 250 microliters of MNase digestion buffer was then added (with protease inhibitor cocktail; Thermo Fisher cat # 78430) to resuspend. MNase (NEB Cat# M0247S, 1 microliter) was then added and cell lysates were mixed by gently pipetting. Samples were then incubated at 37°C for 20 min on an orbital shaker to allow for digestion of chromatin into mono- and di-nucleosomes. 250 microliters 2X stop/ChIP/sonication buffer (100 mM Tris-HCl, pH 8.1, 20 mM EDTA, 200 mM NaCl, 2% Triton X-100, 0.2% Sodium deoxycholate) were added and samples were agitated by vortex mixing. Samples were then sonicated using a Diagenode Bioruptor Pico using 20 total cycles with 30 sec sonication followed by 30 sec rest in each cycle. Samples were then subjected to centrifugation (17,000 X g for 5 min at 4°C), and the supernatant transferred to a new tube. Qubit high-sensitivity assay (Thermo Fisher cat # Q32851) was used to estimate total amount of soluble chromatin. SDS was then added to samples to final concentration of 0.05% to reduce background in subsequent ChIP-experiments. The size of input chromatin fragments were profiled using agarose gel electrophoresis (2% gel).

Chromatin immunoprecipitation and DNA purification

For ChIP reaction, 7 micrograms of prepared chromatin was diluted to a final volume of 450 microliters using 1X ChIP buffer (50 mM Tris-HCl, pH 8.1, 10 mM EDTA, 100 mM NaCl, 1% Triton X-100, 0.1% Sodium deoxycholate) containing 0.05% SDS.

Two micrograms of antibody (H3K4me3 antibody, Abcam cat # ab8580; H3K27me3 antibody, Abcam cat # ab6002; pan-succinyllysine antibody, PTM Biolabs cat # PTM-401; IgG isotype control antibody, Thermo Fisher cat # 02-6102) were then added and samples were rocked overnight at 4°C to allow for antibody binding to chromatin fragments. 0.07 micrograms of input chromatin for each preparation was saved. Following overnight antibody incubation, 30 microliters of pre-washed (300 microliters 1X ChIP buffer) protein G magnetic beads (Pierce Cat#88802) were added to each sample and rocked at 4°C to capture bound chromatin fragments. Samples were then subjected to centrifugation at 700 RPM for 5 min and beads magnetically trapped to facilitate removal of the supernatant. Beads were then washed 2X with 1 mL 1X ChIP buffer, 2X with 1 mL high salt buffer (1X ChIP buffer + 0.5M NaCl), 2X with 1 mL Tris/LiCl buffer (10 mM Tris-HCl, pH 8.0, 0.25 M LiCl, 0.5% NP-40, 0.5% sodium deoxycholate, 1 mM EDTA), and 1 mL TE buffer (50 mM Tris-HCl, pH 8.0, 10 mM EDTA). Beads were resuspended in 50 microliters of 1X ChIP elution buffer (10 mM Tris-HCl, pH 8.0, 10 mM EDTA, 150 mM NaCl, 5 mM DTT, 1% SDS) and incubated at 65°C for 15 min with vortexing performed every 3 min. The eluent was saved in a separate tube and the elution repeated a second time. Both eluents were pooled and incubated at 65°C overnight to reverse formaldehyde cross-links. At this point, the 1% input chromatin sample was diluted into 100 microliters of elution buffer and eluted overnight alongside the ChIP samples. The following day, samples were briefly centrifuged, 2 microliters of RNAse A (Thermo Fisher cat # EN0531) added, samples vortexed to mix, and incubated at 37°C for 1 h to degrade chromatin-associated RNA. 10 microliters of Proteinase K (Ambion cat # AM2546) was then added, samples

vortexed to mix, and then incubated at 37°C for 2 h to degrade chromatin proteins. DNA was purified using Qiagen MinElute columns. Briefly, 500 microliters of Qiagen buffer PB was added to samples, vortexing was performed to mix, samples were loaded onto Qiagen MinElute columns, samples subjected to centrifugation at 9000 RPM for 1 min, eluent discarded, columns washed with 650 microliters of wash buffer, spun to remove residual solvent, and purified DNA eluted with 16 microliters of Qiagen column purification buffer, and subjected to centrifugation at 15,000 RPM for 1 min. Purified DNA was used directly for ChIP-seq deep sequencing library preparation.

ChIP-seq library preparation

Concentration of purified DNA was determined using the Qubit high-sensitivity DNA assay (Thermo Fisher cat # Q32851). Deep sequencing library preparation was performed using 10 ng of purified DNA and the Rubicon Genomics ThruPLEX DNA-seq 48D kit as per the manufacturer's instructions. Libraries were then purified using AMPure XP beads (Beckman Coulter Cat# A63880). Briefly, 50 microliters of beads were combined with each sample and incubated at room temperature for 10 min. Using a magnet, the supernatant was discarded and the beads were washed 2X with 190 microliters of 80% ethanol. Beads were then air dried at 50°C using a heating block, and purified libraries eluted using 21.5 microliters of Qiagen buffer EB at room temperature for 5 min.

Deep sequencing

Deep sequencing was performed by the Mayo Clinic Medical Genome Core Facility using an Illumina HiSeq 4000 instrument, multiplexing 8 bar-coded libraries per lane. Sequencing was performed using 50 cycles and paired end indexed read type.

ChIP-Seq read alignment

FASTA sequences for assembled chromosomes of mouse reference genome GRCm38/mm10 were downloaded from NCBI. Individual chromosomes were concatenated into a single FASTA file, which was used to build Bowtie 2 (version 2.2.3) indices using the “bowtie2-build” function (Langmead and Salzberg, 2012). Paired end read alignments of ChIP-seq FASTQ reads to the indexed mouse reference genome were then performed in Bowtie 2 using default settings on the Mayo Clinic Research Computing Services high performance Beowulf-style Linux-based cluster. The resulting SAM files were converted to BAM format using the Samtools “view” function (Li et al., 2009). BAM files were then sorted by chromosome and region using the Samtools “sort” function, and BAM file indices were generated using the Samtools “index” function.

QUANTIFICATION AND STATISTICAL ANALYSIS

Raw proteomic data processing

MaxQuant (v 1.5.3.12) was used for identification and quantification from MS/MS spectra in the raw data (Cox and Mann, 2008). Lysine succinylation (+100.0160 Da), methionine oxidation and protein N-terminal acetylation were selected as variable modifications. Cysteine carbamidomethylation was selected as a fixed modification. Arginine 6 and Lysine 6 were selected as amino acid labels with three maximum-

labeled amino acids. Trypsin was selected as the proteolytic enzyme and a maximum of two missing cleavages was allowed. The ion mass tolerance for the precursor ion and fragment ion was 4.5 ppm and 0.5 Da respectively. The database search employed the Uniprot mouse database (released on 2013/09/27 and containing 43310 sequences). Peptides were filtered with a 1% False Discovery Rate (FDR) at the peptide, protein and modification site levels. A minimum Andromeda score of 40 was required for the identification of modified peptides. Stoichiometry determination of succinylation sites was achieved following a SILAC-based computational analysis as previously described (Chen, 2016; Olsen et al., 2010). The mass spectrometry proteomics data have been deposited to the ProteomeXchange Consortium via the PRIDE (Vizcaino et al., 2016) partner repository with the dataset identifier PXD007874.

Proteomic data secondary analysis

Secondary analysis of quantified proteomic data was performed in R. SILAC ratios for biological replicate experiments were median-normalized. Analysis of Pearson correlations between replicate experiments or between protein abundance change and succinylation change was performed using the “cor.test” function in R, included in the stats package. Analysis of functional annotation enrichment for differentially succinylated peptides was performed by extracting the gene identifiers for peptides having succinylation $\log_2$(fold-change) differing by more than 0.2 from the corresponding peptide abundance $\log_2$(fold-change). The extracted list of gene identifiers was filtered to remove duplicate gene identifiers, and functional enrichment analysis of gene ontologies (molecular functions, biological processes, and cellular components) and KEGG pathways was performed using the DAVID functional

annotation tool (Huang da et al., 2009). For data display, a criteria was enforced such that all terms must have a p-value < 0.0001 for the enrichment analysis.

ChIP-Seq peak calling and secondary analysis

Secondary analysis of aligned reads was performed in SeqMonk (https://www.bioinformatics.babraham.ac.uk/projects/seqmonk/). Within SeqMonk, the MACS peak calling algorithm was implemented to detect ChIP-seq peaks (p-value cutoff: 1E-5; sonicated fragment size: ~200), comparing mapped read counts for the various ChIP experiments to the corresponding input control (Zhang et al., 2008). Read counts for the various ChIP experiments and input controls were quantified at the positions of ChIP-seq peaks or transcriptions start sites using the feature read count quantitation functionality in SeqMonk. Pearson and Spearman correlations between read counts quantified in the various ChIP experiments was performed in R using the "cor.test" function. For comparisons between signals measured in different types of ChIP experiments, or between ChIP and RNA-seq experiments, data was first scaled in the range of [0,1] using the 0.001 and 0.999 quantiles prior to visualization and analysis of correlation. Analysis of genomic localization of identified ChIP-seq peaks was performed in R using the ChIPseeker package available through the Bioconductor project (Yu et al., 2015). ChIPseeker was also used for generating aligned probe plots and probe trend plots for ChIP-seq peak localization near transcription start sites. For analysis of succinyllysine ChIP peak differential succinylation in the context of SDH loss, peaks were ranked according to observed differences in succinylation (normalized read counts) between experimental and control cell lines. The bottom 0.05 and top 0.95 quantiles of ChIP peaks were extracted, based upon succinylation differences between

experimental and control lines. These subsets of data were then analyzed using ChIPseeker to identify specific types of genomic features impacted by differential succinylation. For analysis of differential promoter succinylation in the context of SDHC loss, promoters genome-wide were ranked according to absolute difference between quantified ChIP-seq read counts in experimental and control samples, and the top 0.1 quantile of differentially succinylated promoters were extracted. The corresponding gene identifiers were extracted and used to perform term enrichment analysis using the DAVID functional annotation database (Huang da et al., 2009). Mean succinylation difference (experimental minus control) for differentially-succinylated genes was calculated in R.

Genotoxic drug study analysis

Amount of reduced Alamar Blue was calculated using the obtained absorbance measurements and the following equation,

$$AR_{570} = A_{570} - (A_{600} X R_o)$$

, where AR570 is the amount of reduced Alamar Blue, A570 and A600 are the absorbance measurements at 570 and 600 nm, respectively, and Ro (0.69) is the empirically-determined ratio of A570 and A600 absorbances for Alamar Blue in media with no cells. Percent difference in Alamer Blue reduction was then determined between drug-treated cells and vehicle-treated cells for each tested cell line.

DATA AND SOFTWARE AVAILABILITY

ChIP-seq data have been deposited in the NCBI GEO under ID code GSE104362. Proteomic data have been deposited in the PRIDE database under ID code PXD007874.

KEY RESOURCES TABLE

REAGENT or RESOURCE	SOURCE	IDENTIFIER
Antibodies		
Rabbit polyclonal IgG isotype control antibody	Thermo Fisher	Cat#02-6102; RRID:AB_2532938
Rabbit polyclonal anti-H3K4me3 IgG antibody	Abcam	Cat#ab8580; RRID:AB_306649
Mouse monoclonal anti-H3K27me3 IgG antibody	Abcam	Cat#ab6002; RRID:AB_305237
Rabbit polyclonal anti-pan-succinyllysine IgG antibody	PTM Biolabs	Cat#PTM-401; RRID:AB_2687628
Bacterial and Virus Strains		
Biological Samples		
Chemicals, Peptides, and Recombinant Proteins		
Doxycycline hyclate	Sigma Aldrich	Cat#D9891-25G
L-Arginine-HCl, 13C6 for SILAC	Thermo Fisher	Cat#88210
Critical Commercial Assays		
ThruPLEX DNA-seq 48D Kit	Rubicon Genomics	Cat#R400406
SILAC protein quantitation kit (LysC), DMEM	Thermo Fisher	Cat#A33969
Qubit dsDNA HS Assay Kit	Thermo Fisher	Cat#Q32851
Deposited Data		
Raw and analyzed ChIP-seq data	This paper	GEO: GSE104362
Raw and analyzed RNA-seq data	Smestad and Hamidi, 2017	GEO: GSE103662
Raw and analyzed proteomic data	This paper	PRIDE: PXD007874
Experimental Models: Cell Lines		
R26M2rtTA/+;TetOcre;Sdhcfl/fl immortalized mouse embryonic fibroblast cell line	Smestad and Hamidi, 2017	N/A
R26M2rtTA/+;TetOcre;Sdhcfl/wt immortalized mouse embryonic fibroblast cell line	Smestad and Hamidi, 2017	N/A

Experimental Models: Organisms/Strains		
Oligonucleotides		
Recombinant DNA		
Software and Algorithms		
Samtools	Li et al., 2009	http://samtools.sourceforge.net/
Bowtie2	Langmead and Salzberg, 2012	http://bowtie-bio.sourceforge.net/bowtie2/index.shtml
SeqMonk	Babraham Bioinformatics	https://www.bioinformatics.babraham.ac.uk/projects/seqmonk/
MACS	Feng and Liu, 2013	http://liulab.dfci.harvard.edu/MACS/
ChIPseeker	Yu, Wang, and He, 2015	http://bioconductor.org/packages/release/bioc/html/ChIPseeker.html
MaxQuant	Cox and Mann, 2008	http://www.biochem.mpg.de/5111795/maxquant
Other		

Supplemental References

Carpenter, A.E., Jones, T.R., Lamprecht, M.R., Clarke, C., Kang, I.H., Friman, O., Guertin, D.A., Chang, J.H., Lindquist, R.A., Moffat, J.*, et al.* (2006). CellProfiler: image analysis software for identifying and quantifying cell phenotypes. Genome Biol *7*, R100.

Chen, Y. (2016). Quantitative Analysis of the Sirt5-Regulated Lysine Succinylation Proteome in Mammalian Cells. Methods in molecular biology *1410*, 23-37.

Cox, J., and Mann, M. (2008). MaxQuant enables high peptide identification rates, individualized p.p.b.-range mass accuracies and proteome-wide protein quantification. Nat Biotechnol *26*, 1367-1372.

Huang da, W., Sherman, B.T., and Lempicki, R.A. (2009). Systematic and integrative analysis of large gene lists using DAVID bioinformatics resources. Nat Protoc *4*, 44-57.

Langmead, B., and Salzberg, S.L. (2012). Fast gapped-read alignment with Bowtie 2. Nat Methods *9*, 357-359.

Li, H., Handsaker, B., Wysoker, A., Fennell, T., Ruan, J., Homer, N., Marth, G., Abecasis, G., Durbin, R., and Genome Project Data Processing, S. (2009). The Sequence Alignment/Map format and SAMtools. Bioinformatics *25*, 2078-2079.

Olsen, J.V., Vermeulen, M., Santamaria, A., Kumar, C., Miller, M.L., Jensen, L.J., Gnad, F., Cox, J., Jensen, T.S., Nigg, E.A.*, et al.* (2010). Quantitative phosphoproteomics reveals widespread full phosphorylation site occupancy during mitosis. Sci Signal *3*, ra3.

Park, J., Chen, Y., Tishkoff, D.X., Peng, C., Tan, M., Dai, L., Xie, Z., Zhang, Y., Zwaans, B.M., Skinner, M.E.*, et al.* (2013). SIRT5-mediated lysine desuccinylation impacts diverse metabolic pathways. Mol Cell *50*, 919-930.

Rappsilber, J., Mann, M., and Ishihama, Y. (2007). Protocol for micro-purification, enrichment, pre-fractionation and storage of peptides for proteomics using StageTips. Nat Protoc *2*, 1896-1906.

Smestad, J., Hamidi, O., Wang, L., Nelson Holte, M., Al Khazal, F., Erber, L., Chen, Y., and James Maher Iii, L. (2017). Characterization and metabolic synthetic lethal testing in a new model of SDH-loss familial pheochromocytoma and paraganglioma. Oncotarget.

Vizcaino, J.A., Csordas, A., Del-Toro, N., Dianes, J.A., Griss, J., Lavidas, I., Mayer, G., Perez-Riverol, Y., Reisinger, F., Ternent, T.*, et al.* (2016). 2016 update of the PRIDE database and its related tools. Nucleic Acids Res *44*, 11033.

Yu, G., Wang, L.G., and He, Q.Y. (2015). ChIPseeker: an R/Bioconductor package for ChIP peak annotation, comparison and visualization. Bioinformatics *31*, 2382-2383.

Zhang, Y., Liu, T., Meyer, C.A., Eeckhoute, J., Johnson, D.S., Bernstein, B.E., Nusbaum, C., Myers, R.M., Brown, M., Li, W.*, et al.* (2008). Model-based analysis of ChIP-Seq (MACS). Genome Biol *9*, R137.

Zhou, T., Chung, Y.H., Chen, J., and Chen, Y. (2016). Site-Specific Identification of Lysine Acetylation Stoichiometries in Mammalian Cells. J Proteome Res *15*, 1103-1113.